[illegible] AND PARTICULATE FORMATION IN [illegible] FUEL FLAMES

[illegible] Bankston, E. Y. Kwack, J. Bellan and K. Harstad

August 15, 1988

Sponsored by

U. S. Army Research Office

ADA201079

UNCLASSIFIED
SECURITY CLASSIFICATION OF THIS PAGE

MASTER COPY - FOR REPRODUCTION PURPOSES

REPORT DOCUMENTATION PAGE

1a REPORT SECURITY CLASSIFICATION Unclassified	1b. RESTRICTIVE MARKINGS
2a. SECURITY CLASSIFICATION AUTHORITY	3 DISTRIBUTION / AVAILABILITY OF REPORT Approved for public release; distribution unlimited.
2b DECLASSIFICATION / DOWNGRADING SCHEDULE	
4 PERFORMING ORGANIZATION REPORT NUMBER(S)	5 MONITORING ORGANIZATION REPORT NUMBER(S) ARO 21092.6-EG
6a. NAME OF PERFORMING ORGANIZATION Jet Propulsion Laboratory California Institute of Tech. — 6b OFFICE SYMBOL (If applicable)	7a. NAME OF MONITORING ORGANIZATION U. S. Army Research Office
6c. ADDRESS (City, State, and ZIP Code) 4800 Oak Grove Drive Pasadena, CA 91109	7b. ADDRESS (City, State, and ZIP Code) P. O. Box 12211 Research Triangle Park, NC 27709-2211
8a. NAME OF FUNDING / SPONSORING ORGANIZATION U. S. Army Research Office — 8b. OFFICE SYMBOL (If applicable)	9. PROCUREMENT INSTRUMENT IDENTIFICATION NUMBER MIPR 109-86, NASA
8c. ADDRESS (City, State, and ZIP Code) P. O. Box 12211 Research Triangle Park, NC 27709-2211	10. SOURCE OF FUNDING NUMBERS PROGRAM ELEMENT NO / PROJECT NO / TASK NO / WORK UNIT ACCESSION NO

11 TITLE (Include Security Classification)

Investigation of Spray Dispersion and Particulate Formation in Diesel Fuel Flames

12 PERSONAL AUTHOR(S) L. H. Back, C. P. Bankston, E. Y. Kwack, J. Bellan and K. Harstad

13a. TYPE OF REPORT	13b TIME COVERED	14 DATE OF REPORT (Year, Month, Day)	15 PAGE COUNT
Final	FROM 83/12/2 TO 88/6/30	1988, August 15,	79

16. SUPPLEMENTARY NOTATION The view, opinions and/or findings contained in this report are those of the author(s) and should not be construed as an official Department of the Army position, policy, or decision, unless so designated by other documentation.

17 COSATI CODES		
FIELD	GROUP	SUB-GROUP

18 SUBJECT TERMS (Continue on reverse if necessary and identify by block number)
diesel fuel jets, electrostatic spray dispersion, combustion

19 ABSTRACT (Continue on reverse if necessary and identify by block number) An experimental study of electrostatically atomized and dispersed diesel fuel jets was conducted at various back pressures to 40 atm. A new electrostatic injection technique was utilized to generate continuous, stable fuel sprays at charge densities of 1.5 - 2.0 C/m^3 of fluid at one atm, and about 1.0 C/m^3 at 40 atm. Flow rates were varied from 0.5 to 2.5 ml/s and electric potentials to -18 kV. Visual observations showed that significant enhanced dispersion of charged fuel jets occurred at high back pressures compared to aerodynamic breakup and dispersion. The average drop size was about the same as the spray triode orifice diameter, and was between the Kelly theory and the Rayleigh limit. The ignition tests, done only at one atm, indicated stable combustion of the electrostatically dispersed fuel jets. Theoretical modeling of the evaporation and dispersion of a spherical cluster of charged drops moving in an ambient gas indicated that the charge acts to expand a dense cluster of drops into the hot ambient gas, thus promoting evaporation. The experimental results are encouraging for engine injection, but more research is needed to evaluate the potential for improvement in combustion and reduced soot formation.

20 DISTRIBUTION / AVAILABILITY OF ABSTRACT	21. ABSTRACT SECURITY CLASSIFICATION
☐ UNCLASSIFIED/UNLIMITED ☐ SAME AS RPT. ☐ DTIC USERS	Unclassified
22a NAME OF RESPONSIBLE INDIVIDUAL	22b. TELEPHONE (Include Area Code) / 22c. OFFICE SYMBOL

DD FORM 1473, 84 MAR — 83 APR edition may be used until exhausted. All other editions are obsolete.

SECURITY CLASSIFICATION OF THIS PAGE
UNCLASSIFIED

JPL D-5704

INVESTIGATION OF SPRAY DISPERSION AND PARTICULATE FORMATION IN DIESEL FUEL FLAMES

FINAL REPORT

L. H. Back, C. P. Bankston, E. Y. Kwack, J. Bellan and K. Harstad

August 15, 1988

Sponsored by

U. S. Army Research Office

MIPR 109-86, NASA

Jet Propulsion Laboratory
California Institute of Technology
Pasadena, CA 91109

Prepared by the Jet Propulsion Laboratory, California Institute of Technology, for the U.S. Army Research Office through an agreement with the National Aeronautics and Space Administration.

The work reported herein was performed through NASA Task RE-182, Amendment 349, and was sponsored by the U.S. Army Research Office under MIPR 109-86.

Table of Contents

		Page
I.	INTRODUCTION	1
II.	RESULTS	2
	Experimental	2
	Theoretical Modeling	4
III.	REFERENCES	6

Papers resulting from this investigation.

A. Bankston, C. P., Back, L. H., Kwack, E. Y., and Kelly, A. J., "Experimental Investigation of Electrostatic Dispersion and Combustion of Diesel Fuel Jets," ASME J. Engrg. for Gas Turbines and Power., Vol. 110, No. 3, July, 1988, pp. 361-368.

B. Kwack, E. Y., Back, L. H., and Bankston, C. P., "Electrostatic Dispersion of Diesel Fuel Jets at High Back Pressure," to be presented at the Western States Section/The Combustion Institute, Laguna Beach, CA, October, 1988; and to be submitted for publication.

C. Bellan, J. and Harstad, K., "The Details of the Convective Evaporation of Dense & Dilute Clusters of Drops," Int. J. Heat Mass Transfer, Vol. 30, No. 6, 1987, pp. 1083-1093.

D. Bellan, J., and Harstad, K., "Turbulence Effects During Evaporation of Drops in Clusters," Int. J. Heat Mass Transfer, Vol. 31, No. 8, August, 1988, pp. 1655-1668.

E. Harstad, K., and Bellan, J., "Electrostatic Dispersion of Drops in Clusters," to be presented at the 22nd Int. Sym. on Combustion, Seattle, WA, August, 1988; and submitted for publication.

APPENDICES I and II.

I. INTRODUCTION

Military diesel engines are widely utilized in vehicles and for mobile and stationary power generating plants. Uncertainties in fuel resources and variability in fuel costs require that future diesel engines operate with improved efficiencies while maintaining low smoke emissions with fuel that may be low in quality. Thus, a better understanding of fuel injection and combustion processes in diesel combustion chambers is needed and strategies to improve performance are desired.

Combustion in diesel engines is significantly affected by fuel spray injection and flow characteristics (Heinein[1]). Many methods for improved mixing and dispersion of the spray to reduce local fuel rich regions have been investigated for improved combustion and reduced soot formation. In general, the breakup of fuel jets in diesel engines is accomplished by high pressure injection in the range 20 MPa, 200 atm (for indirect injection) up to about 140 MPa, 1400 atm (for direct injection). The mechanism of breakup of a fuel jet at high velocity injection has been investigated and reviewed by Reitz and Bracco[2] and Lin and Kang[3]. Swirl is imparted to the flow field in the chamber to further assist the fuel-air mixing process, and soot formation is strongly dependent upon swirl characteristics. However, fuel-rich regions apparently still persist in current engines, and methods for improved mixing and reduced soot formation continue to be of interest.

Techniques for improving in-cylinder combustion characteristics include mechanical, chemical, and electrical methods. Mechanical methods include the adjustment of injection timing and changes in injection geometries (Pischinger and Cartellieri[4]; Khan et al[5]). Chemical concepts usually rely upon fuel additives or the application of catalysts on cylinder surfaces (Gaffney et al[6]). Recently, studies of microexplosions in fuel-water and fuel-alcohol mixtures have led to the possibility that such a breakup process could be utilized to enhance dispersion of the injected fuel (Wang and Law[7]). Electrical concepts have been based on observed electrical phenomena in the combustion process. Electrical fields have been applied to the combustion chamber (Ahmad et al[8]; Miller et al[9]) however, the fundamental phenomena was not studied. Also plasma devices have been proposed to enhance the combustion process.

The concept studied in this investigation involves the injection of a fuel jet that is electrostatically broken up and dispersion enhanced by the repulsion of like-charged droplets. Numerous attempts have been made to develop

electrostatic fuel atomizers for use in combustion systems and also to develop models to explain the electrostatic processes of breakup and dispersion of fuel jets, and those investigations were reviewed by Kelly[10]. However, electrostatic dispersion of a fuel spray has not proven practical due to the very high resistivities of liquid hydrocarbon fuels (10^{10} - 10^{12} ohm-m) (Kelly[10,11]; Luther[12]) which presents difficulties in producing electrostatically charged sprays at flow rates above 0.1 mℓ/s (Luther[12]; Newgard and Noon[13]). The electrostatic spray device conceived and demonstrated by Kelly[10,11] has overcome many of these previous limitations. This Spray Triode can charge mineral oil Marcol-87 (viscosity = 25 cp) up to 1.8 C/m^3 for flow rates up to 1.25 mℓ/s (Kelly[10]).

The objectives of this research were to investigate experimentally the characteristics of charged diesel fuel jet atomization, dispersion and combustion, and to theoretically model dispersion and evaporation of charged fuel sprays.

II. RESULTS

The results of this investigation are reported in a series of papers Refs. A-E listed in the Table of Contents. Refs. B and E are included as Appendices in this report since they have not been published yet. These papers are briefly described and the important results are summarized as follows.

Experimental

Ref. A presents results obtained at one atmospheric pressure and room temperature. In this work a Spray Triode with two orifice sizes, 173 and 422 μm was tested at steady flow rates of 0.25-1.0 mℓ/s with mineral oil (viscosity ≃ 25 cp) under non-combusting conditions, and with no. 2 diesel fuel (viscosity ≃ 6 cp) under combusting and non-combusting conditions. The experimental setups for the noncombusting and combusting experiments are shown in Fig. 5 of Ref. A, along with a detailed diagram of the Spray Triode, Fig. 6. Spray charge densities were determined by measuring the current carried by the fluid with an electrometer in series between the collector electrode and ground. Charge density was determined by dividing the electric current by the measured liquid volume flow rate. Characterization of the spray was carried out by flash illumination and photography. Analysis of the spray pictures was carried out using an image processing system.

The results from Ref. A are summarized as follows:

1. Continuous, stable fuel sprays were generated with charge densities of 1.5 - 2.0 C/m^3 of fluid.
2. Calculations using a model proposed by Bellan[14] showed that such charge densities may enhance spray dispersion under diesel engine conditions.
3. Measured mean drop diameters were near 150 μm, being between Kelly's statistical equilibrium end state model[10,15] and the Rayleigh limit.
4. The electrical power required to generate these sprays was less than 10^{-6} times the chemical energy available from the fuel.
5. The results showed considerable differences in spray characteristics between a diesel injector (also studied) and electrostatic injection.
6. Ignition and stable combustion of electrostatically dispersed diesel fuel jets were achieved.

Ref. B (Appendix I) presents recent results obtained at various back pressures to 600 psig using a spray triode designed by the Parker Hannifin Company to fit into a small Volkswagon diesel engine. This spray triode has a 254 μm diameter orifice and can be operated up to a fuel pressure of 3000 psig, electric potentials of -20 kV and temperatures of 200°C. The experiments were conducted in a high pressure chamber with a relatively large window to allow spray development to be observed (Fig. 1, Ref. B). Provision was also made to measure the total current to the cathode i_t and the collector current i_f (charge carried by the fuel per unit time) by using a switching arrangement. The electric charge density of the diesel spray was measured over a range of flow rates from 0.5 to 2.5 mℓ/s at various chamber pressures of 0, 300 and 600 psig by applying different electric potentials to -18 kV. Characterization of the spray was carried out by flash illumination and photographs with and without applied electric fields at fuel injection velocities of 20 and 40 m/s, and at various voltages. Droplet sizing by image processing was done for the data at a chamber pressure of 300 psig.

The results from Ref. B are summarized as follows:

1. The average charge density of fuel drops linearly increased up to 1.5 C/m^3 with increasing electric potential until breakdown occurred.
2. After breakdown the charge density was reduced by 40 to 60% and again increased with a smaller slope as the electric potential was increased.
3. At higher flow rates breakdown occurred at higher voltages.

4. At high back pressure lower charge density was obtained (about 1 C/m^3 at 600 psig) and breakdown occurred at higher voltages.
5. In general, with electric charge rapid breakup of the jet was achieved without large droplets in the core region.
6. The spray angle increased to about 180 deg. with increase of electric potential which enhanced dispersion of the fuel near the nozzle exit and reduced the dense core region.
7. It was observed that the size of drops may be determined by the charge density rather than aerodynamic forces.
8. The average drop size was about the same as the spray triode orifice diameter and was between the Kelly theory and the Rayleigh limit.

In conclusion, these experimental investigations show that electrostatic fuel injection can be achieved at practical flow rates, and that significant early breakup and dispersion of charged fuel jets occur at high back pressures compared to aerodynamic breakup and dispersion. These results are encouraging for engine injection, but demonstration of this electrostatic technique under pulsed fuel injection and autoignition conditions requires subsequent investigations to evaluate the potential for improvement in combustion and reduced soot formation. Since we have experienced recurrent failure of the insulation in the high pressure electrostatic spray triode, a more durable unit is also needed.

Theoretical Modeling

In Ref. C and D a model of convective spray evaporation has been developed for dense and dilute clusters of drops. The model is for a cluster of monodisperse, single component, spherical drops that is exposed to a surrounding convective gas flow. The model takes into account droplet interactions within the cluster and the resulting limitations on evaporation as fuel vapor accumulates within the cluster. Results obtained from this model appear in Ref. C and D and, are not summarized here. This work was jointly supported by the Army Research Office, the U. S. Dept of Energy/Energy Conversion and Utilization Technology Program, and the Air Force Office of Scientific Research/Directorate of Aerospace Sciences.

The model formulation for the evaporation of a cluster of monodisperse fuel drops was extended more recently to include the effects of drop charge. Two

different geometries were considered: (1) a spherical cluster of drops traveling in an ambient gas, and evolving in time, and (2) a steady axisymmetric jet spray flow where axial distance corresponds to time (Lagrangian coordinate). The momentum equations for drops and gases were generalized to account for drop slip and radial cluster expansion. Combined with the momentum equations, the cluster energy equation becomes the determinant for cluster radius. When the drop Rayleigh limit is reached (drop instability due to charge), the calculation is stopped since the remaining mass of the drops is negligible for the sizes of drops of interest.

Results obtained for the evaporation and dispersion of a spherical cluster of charged drops moving in an ambient gas are given in Ref. E. (Appendix II) For dense clusters of drops, it was found that electrostatic effects dominated, and that turbulence effects, modeled as described in Ref. D, were not the controlling parameter as was the case for uncharged drops. The charge acts to expand a dense cluster of drops into the hot ambient gas, thus promoting evaporation. For dilute clusters of drops, neither electrostatic nor turbulence effects were important. Based upon single-droplet-stream experiments by Sangiovanni and Liscinsky[16] and the results of the calculations, inferences were made about how electrostatic spray dispersion may reduce the soot emission index by increasing drop spacing. Also, limited results pertaining to the ignition of nearly-dense clusters of electrostatically charged drops were discussed.

The case of a jet flow of charged drops has been formulated, but has not been programmed for numerical calculations. This would require a subsequent study to obtain information on dispersion and evaporation effects in a geometry more like in our experiments.

III. REFERENCES

1. Heinein, N. A., (1976), "Analysis of Pollutant Formation and Control and Fuel Economy in Diesel Engines," Prog. Energy Combust. Sci., Vol. 1, pp. 165-207.

2. Reitz, R. D. and Bracco, F. V., (1982), "Mechanism of Atomization of a Liquid Jet," Physics of Fluids, Vol. 25, No. 10, pp. 1730-1742.

3. Lin, S. P. and Kang, B. J., (1987), "Atomization of a Liquid Jet," Physics of Fluids, Vol. 30, No. 7. pp. 2000-2006.

4. Pischinger, R. and Cartellieri, W., (1972), "Combustion System Parameters and Their Effect Upon Diesel Engine Exhaust Emissions," SAE paper No. 720765.

5. Khan, I. M., Wang, C. H. T., and Langridge, B. E., (1972), "Effect of Air Swirl on Smoke and Gaseous Emissions from Direct-Injection Diesel Engines," SAE paper No. 720102.

6. Gaffney, J., Sapieza, R., Butcher, T., Drishna, C., Marlow, W., and O'Hare, T., (1980), "Soot Reduction in Diesel Engines: A Chemical Approach," Combustion Science and Technology, Vol. 24, pp. 89-92.

7. Wang, C. H., and Law, C. K., (1985), "Microexplosion of Fuel Droplets Under High Pressure," Combustion and Flame, Vol. 59, pp. 53-62.

8. Ahmad, T., Speck, C. E., and Sing, D. C., (1980), "Effect of Electric Fields Applied Within the Prechamber on Particulate Emissions from a Diesel Engine," presented at the Fall Technical Meeting, Western States Section, Combustion Institute, General Motors Research Report No. GMR-3326, October.

9. Miller, J. A., Biblarz, O., Zajdman, A., Manning, W. W., II, and Mavroudis, J. A., (1987), "Electrostatic Spray Modification in Gas Turbulent Combustion," J. Propulsion and Power, Vol. 3, No. 2, pp 187-192.

10. Kelly, A. J., (1982), "The Electrostatic Atomization of Hydrocarbons," Proceedings of the 2nd Int. Conf. on Liquid Atomization and Spray Systems, June.

11. Kelly, A. J., (1981), "Electrostatic Atomizing Device," U. S. Patent No. 4,255,777, March 10.

12. Luther, F. E., (1962), "Electrostatic Atomization of No. 2 Heating Oil," Proc. 2nd API Research Conference on Distillate Fuel Combustion, API Publication No. 1701, June.

13. Newgard, P. M. and Noon, A. W., (1964), "Electrostatic Atomizer and Burner Research," Distillate Fuel Combustion Conference, API Publication No. 1725, November.

14. Bellan, J., (1983), "A New Approach to Soot Control in Diesel Engines by Fuel-Drop Charging," Combust. Flame, Vol. 51, pp. 117-119.

15. Kelly, A. J., 1978, "Electrostatic Spray Theory," J. Applied Physics, Vol. 49, pp. 2621-2628.

16. Sangiovanni, J. J. and Liscinsky, D. S., 1984, "Soot Formation Characteristics of Well-Defined Spray Flames," Proc. of the 20th Symp. (Int.) on Combustion, pp. 1063-1073.

Appendix I

ELECTROSTATIC DISPERSION OF DIESEL FUEL JETS AT HIGH BACK PRESSURE

E. Y. Kwack[+], L. H. Back[++] and C. P. Bankston[+]

Jet Propulsion Laboratory
California Institute of Technology
Pasadena, CA 91109

ABSTRACT

An experimental study of electrostatically atomized and dispersed fuel jets has been conducted for various back pressures to 600 psig. No. 2 diesel fuel was injected through an electrostatic spray triode designed for a small diesel engine. Charge density measurements were conducted at various combinations of injection velocities, electric potentials and back pressures. The charge density of fuel drops linearly increased up to 1.5 C/m^3 with increasing electric potential until breakdown occurred. After breakdown the charge density was reduced by 40 to 60 % and again increased with a lower slope as electric potential increased. At higher flow rates, breakdown occurred at higher voltages. At higher back pressure, lower charge density was obtained and breakdown occurred at higher voltages. Visual observation showed that significant electrostatic dispersion was accomplished at high back pressures, and that the average drop size was about the same as the spray triode orifice diameter.

I. INTRODUCTION

Diesel engines are widely used for transportation vehicles and power generation. Unfortunately, one of their important drawbacks is the fact that they produce non-negligible amounts of soot. The soot is formed in the fuel rich regions of the spray where a large amount of fuel vapor accumulates without burning and undergoes pyrolysis reactions which transforms it to soot. Mixing and controlled atomization have good potential to reduce soot yield in spray flames (Prado et al, 1977). Many methods for improved mixing and dispersion of the spray to reduce local fuel rich regions have been investigated for improved combustion and reduced soot formation.

In general, the breakup of fuel jets in diesel engines is accomplished by high pressure injection in the range 20 MPa, 200 atm (for indirect injection) up

+Associate Member, ASME
++Fellow, ASME

to about 140 MPa, 1400 atm (for direct injection). The mechanism of break up of a fuel jet at high velocity injection has been investigated and was well reviewed in articles by Reitz and Bracco (1982) and Lin and Kang (1987). Swirl is imparted to the flow field in the chamber to further assist the fuel-air mixing process, and soot formation is strongly dependent upon swirl characteristics. However, fuel rich regions apparently still persist in current engines, and methods for improved mixing and reduced soot formation continue to be of interest.

Techniques for improving in-cylinder combustion characteristics include mechanical (Pischinger and Cartellieri, 1972; Khan et al, 1972), chemical (Gaffney et al, 1980) and electrical methods. Electrical concepts involve the injection of a fuel jet which is electrostatically broken up and dispersion enhanced by the repulsion of like-charged droplets. Numerous attempts have been made to develop electrostatic fuel atomizers for use in combustion systems and also to develop models to explain the electrostatic processes of breakup and dispersion of fuel jets, and those investigations were reviewed by Kelly (1982). However, electrostatic dispersion of a fuel spray has not proven practical due to the very high resistivities of liquid hydrocarbon fuel (10^{10} - 10^{12} ohm-m) (Kelly, 1981, 1982; Luther, 1962) which presents difficulties in producing electrostatically charged sprays at flow rates above 0.1 mℓ/s (Luther, 1962; Newgard and Noon, 1964). The electrostatic spray device conceived and demonstrated by Kelly (1981, 1982) has overcome previous limitations and can charge mineral oil Marcol-87 (viscosity = 25cp) up to 1.8 C/m^3 for flow rates up to 1.25 ml/s. The detailed schematic diagram of the spray triode can be found in Refs. (Kelly, 1982; Bankston et al. 1988). Bankston et al (1988) used a spray triode provided by Kelly and obtained charge densities of 1.5 - 2.0 C/m^3 for a

mineral oil and diesel fuel oil. Of note is that both the experimental studies by Kelly (1982) and Bankston et al. (1988) were conducted at ambient back pressure. No experimental study has been conducted with this kind of triode for high back pressures.

Bankston et al. (1988) also estimated the effect of charged droplets on the dispersion of a spherical cluster of fuel drops under diesel engine conditions using a model proposed by Bellan (1983) based on a model of evaporation of dense clusters of drops (Bellan and Cuffel, 1983). That model predicts the expansion of an initially spherical droplet spray cloud of radius R_0, due to the repulsion of uniformly charged and distributed droplets. Bankston et al (1988) has calculated spray cloud dispersion versus charge density in 0.5 ms; for example, a spherical spray volume 1 cm in radius and containing 54 mg of diesel fuel will expand by a radius factor of 1.4 in 0.5 ms at a charge density of 2 C/m^3. Although the model does not account for drag effects and is developed for a spherical spray cluster, not for a cylinderical plume like a spray jet from a nozzle, the results indicate that the electrostatic dispersion can be considered promising to control or reduce soot formation. A simple model of electrostatic spray plumes was developed by True (1983) but no account was taken of droplet evaporation and droplet interactions due to their near proximity. Harstad and Bellan (1988) proposed a more complex model for a spherical cluster of charged drops by extending their model for evaporation of dense clusters of fuel drops (Bellan and Harstad, 1987, 1988) to acccunt for electrostatic effects.

Electrostatic spray concepts have been applied to the actual combustion chamber (Ahmad et al, 1980; Miller et al, 1987) however, there was a lack of study of the fundamental phenomena. Moreover, not much experimental work has been done at high back pressure. With this as a background, this detailed

experimental study was carried out to investigate the effects of high back pressure on the charging of fuel jets and the behavior of breakup and dispersion of charged fuel drops.

II. EXPERIMENTAL SETUP

The nozzle used in the current study is the first electrostatic spray triode (EST) "single hole" injector designed by Parker Hannifin Company to fit into a Volkswagen diesel four-cylinder engine of nominal 48 horsepower output. The basic operational principle of the EST nozzle can be found in previous reports (Kelly, 1982; Bankston et al., 1988). The OMC (Oxide-Metal Composites) company manufactured the insulator-electrode (emitter) assembly and Parker Hannifin Company assembled it into the housing. Any diesel fuel or fuel simulant can be used in this EST nozzle as long as the fluid is non-conducting and has similar electrical properties as diesel fuel. The EST nozzle has a 254 μm diameter orifice and can be operated up to fuel pressures of 3000 psig, electric potertials of 20 kV and temperatures of 200^{o}C.

The EST was located in the top of a high pressure chamber 15 cm I.D. and 40 cm height which also has a 10 cm diameter window to allow spray development to be observed (Fig. 1). The EST injects fuel vertically downward into a cylinderical glass container of 10 cm diameter and 25 cm height placed inside the high pressure chamber. The glass container is lined with copper wire screen on the wall and has copper gauze on the bottom in order to collect the charge of the dispersed fuel spray.

The copper wire screen and gauze are connected to an electrometer to measure the electric charge carried by the fuel per unit time i_f which when divided by the volume flow rate $\dot{Q}$ gives the mean charge density ρ_e.

$$\rho_e = i_f/\dot{Q} \tag{1}$$

The fuel, charged by cathode emissions, either goes to the anode/orifice electrode or is swept downstream to the collector. Therefore, the total charge per unit time i_t is the sum of the charge carried to the anode and to the collector per unit time.

$$i_t = i_a + i_f \tag{2}$$

The anode is connected to the electrometer as shown in Fig. 1 by a switching arrangement when the total current is measured.

The high pressure chamber was pressurized up to 600 psig by N_2 gas. Fuel is supplied to the EST nozzle by the pressure difference between the fuel tank and the high pressure chamber through a line with a 10 μm filter to remove particles which can cause the nozzle to plug, to spray erratically, and to lead to early electrical breakdown. The flow rates through the EST were calibrated as a function of pressure difference measured using a differential pressure transducer for three different chamber pressures of 0, 300 and 600 psig. It was found that the calibration was almost independent of the chamber pressure. Since it was planned to increase the pressure inside the chamber to 600 psig to simulate the pressure inside a small diesel engine cylinder before the injection of fuel, the high pressure chamber and the fuel tank were located in one room for safety and the associated instrumentation was located in an adjacent control room. For remote control, a solenoid valve was located in the fuel line between the 10 μm filter and the EST nozzle.

The test fluid was No. 2 diesel fuel with a viscosity of about 6cp. The density and the surface tension of No. 2 diesel fuel are 0.824 g/cm^3 and 30 dyne/cm, respectively. The electric charge density of the diesel spray was measured for various flow rates/injection velocities at various chamber pressures of 0, 300 and 600 psig by applying different electric potentials with a power supply.

Characterization of the spray was carried out by flash illumination and photographs. Analysis of the photographs was carried out using an image processing system. A photograph was placed on a light table in view of a video camera (Model CC-65S, DAGE-MTI, Inc). The analog signal from the video camera was fed to a digitizer which writes the data into RAM memory using an add-on board (PCvision Frame Grabber, Imaging Technology) in conjunction with an IBM PC-AT. A computer code was developed with the aid of commercially available software (IMAGELAB/IMAGETOOL, Werner Frei Associates) for image enhancement and analysis of droplet size.

III. RESULTS AND DISCUSSION

1. Electric Charge Density

The amounts of charge emitted by the cathode and that swept downstream per unit time, i_t and i_f, respectively, were measured for a wide range of the flow rate at p_c = 0 psig by a switching arrangement. The results of i_t and i_f for a fixed flow rate $\dot{Q}$ = 1.2 mℓ/s are shown in Fig. 2 as a function of the electric potential. The cathode starts emitting electrons from its surface if the local electric field is higher than the minimum value needed to extract electrons from metallic surface which is of the order of 10^9 V/m. The number of electrons

emitted from the cathode per unit time is proportional to the strength of the l al electric field above the minimum value at a given fuel flow rate (Fig. 2).

Once the electrons are injected into the fuel, they are coupled with the fuel near the cathode, forming a charged cloud or layer. Some of the charged fuel is attracted to the anode/orifice electrode (i_a) and the other is discharged to the collector (i_f) as shown in Fig. 2. The amount of charge attracted to the orifice electrode depends on electron mobilities of the charged fuel which are in the range of 10^{-7} to 10^{-8} $m^2/V.sec$ (Inuishi, 1979). Therefore, more charged fuel is attracted to the orifice electrode as the electric field increases (Fig. 2). If the fuel velocity or flow rate increases at a fixed electric potential, more charged fuel in the layer moves downstream (Fig. 3) and the charged layer becomes thinner which results in more emission of electrons from the cathode. In other words, the total charge emitted from the cathode increases with increasing flow rate (not shown) like the charge carried downstream does (Fig. 3).

The layer of the charged fuel becomes thicker as the electric field increases, until it reaches the anode locally and forms an electric channel or low conducting path, so-called electric breakdown. After elecric breakdown occurs, the amount of electrons emitted by the cathode increases drastically by 5 to 10 times (Fig. 2). However, since most electrons move to the anode directly, and are not carried by the fuel, the amount of electrons emitted by the cathode no longer depends on the fuel flow rate. At the same time, most of the electrons are attracted to the anode and only a small amount is swept away by the fuel so that i_f is reduced by 40 to 60 % after breakdown (Figs. 2 and 3). The ratio of the charge swept downstream to the total emitted charge was observed to be 0.1 to 0.5 for the range of flow rates 0.4 to 1.8 $m\ell/s$ before breakdown occurred. After breakdown, the ratio was reduced below 0.05. After breakdown i_t and i_f again

increase gradually as electric potential increases. However, the slope of i_f is much lower than that before breakdown while the slope of i_t remains the same. Therefore, the ratio decreases as electric potential increases after breakdown. Since the rate of growth of the charged layer decreases as the fuel velocity increases, breakdown occurs at higher voltages, -8.5 kV at 0.51 mℓ/s to -13 kV at 2.5 mℓ/s (Fig. 3).

The maximum amount of charge on a liquid drop is limited by the Rayleigh relation:

$$\rho_{e_{max}} = 12(2\varepsilon_0\gamma)^{1/2}d^{-1.5} \qquad (3)$$

If the charge increases more than the maximum limit, the liquid drop would breakup into several small drops. Therefore, the charge density $\rho_{e_{max}}$ is an important parameter in determining the largest drop size.

The experimental results shown in Fig. 3 were converted to charge density by dividing i_f by the flow rate $\dot{Q}$ and the results are shown in Fig. 4. The charge per unit time carried by the fuel to the collector, i_f, increased with increasing flow rate to 2 mℓ/s at a fixed voltage before breakdown occurred (Fig. 3). However, the incremental increase was not enough to give the same or larger charge density, so that the charge density monotonically decreased with increasing flow rate. However, the maximum charge density which was obtained just before electrical breakdown occurred is 1.0 C/m³ at the flow rate of 0.51 mℓ/s and increases with increasing flow rate, reaching a peak value of 1.53 C/m³ at a flow rate of 1.5 mℓ/s. Further increase of the flow rate resulted in a slight decrease of the maximum charge density.

Since the chamber pressure in a diesel engine before fuel injection is relatively large, the charge density of No. 2 diesel fuel was measured for high

back pressures up to 600 psig (at 300 and 600 psig) and the results are shown in Figs. 5 and 6. The results for the high back (chamber) pressures exhibit similar behavior as those at p_c = 0 psig i.e. the charge density increases with an increase of the applied voltage at a fixed flow rate, and decreases with increasing flow rate at a fixed applied voltage. The chamber pressure, however, plays an important role in determining the charge density and the breakdown voltage. Breakdown seems to occur at a higher voltage for a fixed flow rate as the chamber pressure increases. For example, for $\dot{Q}$=0.51 mℓ/s the breakdown occurs at E=-8.5 kV for p_c = 0 psig, at E =-10 kV for p_c = 300 psig and at E=-11 kV for p_c = 600 psig. The decrease in the charge density right after breakdown is much smaller for higher chamber pressures. The charge density decreases by 20% for p_c = 300 and 600 psig, compared to 50% for p_c = 0 psig at $\dot{Q}$ = 0.51 mℓ/s. Moreover, the charge density decreases as the chamber pressure increases before breakdown occurs, if the flow rate and the applied voltage are the same. This behavior is clearly seen in Fig. 7 which shows the charge density as functions of the flow rate at E = -8 kV for p_c = 0, 300 and 600 psig. The charge density at p_c = 0 psig is about 1 C/m³ at $\dot{Q}$ = 0.51 mℓ/s and monotonically decreases with increase of the flow rate, reaching about 0.3 C/m³ at $\dot{Q}$ = 2.5 mℓ/s. The charge densities at pressures of 300 and 600 psig show similar behavior but, however, are smaller than those at 0 psig by 10 - 17% for 300 psig and 40 - 50 % for 600 psig, depending on the flow rate.

The maximum charge densities measured at three different back pressures are plotted in Fig. 8 using the results shown in Figs. 4, 5 and 6. This plot clearly demonstrates that the maximum charge density becomes smaller as the back pressure increases if the electric potential is limited, i.e. E = -14 kV. The maximum

charge density is smaller by 20 - 26% at 300 psig and by 22 - 43% at 600 psig depending on flow rate, compared to that at 0 psig.

The detailed maximum charge density with the high pressure spray triode was measured at two different chamber pressures p_c of 0 and 300 psig for a wider range of flow rates of 0.3 to 4.2 mℓ/s. In this case, the electric potential was applied to -18kV. The maximum charge density increases with increasing the flow rate, reaching maximum values of 1.65 C/m³ at p_c = 0 psig and 1.5 C/m³ at p_c = 300 psig as shown in Fig. 9. It remained at the maximum value for a range of flow rates and tended to decrease with further increase of flow rate. The maximum charge density at 300 psig was lower than that at 0 psig by 10-25%, depending on flow rate.

The electrostatic spray triode used in the current study shows different characteristics at low flow rates compared to those used by Kelly (1982) and Bankston et al (1988) for atmospheric pressure. For example, Kelly reported almost constant charge density of 1.5 C/m³ for a range of flow rates from 0.25 to 1.25 mℓ/sec. However, the charge density in Fig. 9 almost increases linearly up to flow rates of 1.5 mℓ/s at 0 psig and 2.2 mℓ/s at 300 psig, and then remains constant. In any case, the data confirm that charge densities of 1.5 C/m³ up to a flow rate of 4.3 mℓ/s are definitely achievable at atmospheric pressure, and slightly lower values are found at high pressures. The performance at high pressure may be improved by redesigning the insulator which limits the electric potential. If an electrostatic spray triode were used in a diesel engine, the applied voltage should be varied according to the injected fuel amount or injection velocity since the maximum charge density is obtained at higher electric field as the flow rate increases.

2. Flow Visualization

Pictures were taken of diesel fuel injected through the high pressure spray triode. Photos were taken through the 10 cm I.D. window at various combinations of test conditions of chamber pressure, fuel injection velocity and applied voltages as shown in Table 1.

Table 1.

pressure, psig	V_i = 20 m/s	V_i = 40 m/s
0	0, -8, -10kV	0, -8, -10kV
300	0, -10, -12kV	0, -10, -12kV
600	0kV	0kV

Without Electric Charge

When fuel was injected into air at 0 psig (atmospheric pressure) a single stream of fuel was observed all the way across the window without electric charge even at an injection velocity of 40 m/s (Fig. 10a). At p_c = 300 psig, V_i = 20 m/s, the fuel jet breaks up even without the applied voltage since the nitrogen density is about 21 times larger than that of air at atmospheric pressure (Fig. 10b). The fuel jet begins breaking up at 0.75 cm beyond the injection nozzle (x_1/d_n = 30) and mixes with surrounding nitrogen gas, forming a spray plume having an included angle of 26°. However, a dense central core exists for several centimeters beyond the injection nozzle. Many large irregular droplets were observed to remain in this dense core region. When fuel is injected at 40 m/s (Fig. 10c), the jet breaks up earlier, less than 0.5 cm beyond the nozzle exit, forms a narrow spray angle of 23°, and breaks up into much smaller

droplets. The fuel was also injected into nitrogen gas having a pressure of 600 psig to simulate an actual diesel engine. Compared to data at 300 psig, spray angles are larger and the jet breaks up earlier: $\theta = 35^0$, $x_1 = 0.5$ cm at 20 m/s (Fig. 10d) and $\theta = 30^0$, $x_1 = 0$ cm at 40 m/s (Fig. 10e). The droplet sizes are somewhat larger at 600 psig if the injection velocity is the same. Despite the large spray angle at $p_c = 600$ psig, the dense core still exists for several centimeters beyond the injector nozzle.

Atomization of fuel jets has been studied using aerodynamic interaction mechanisms (Ranz, 1958; Reitz and Bracco, 1982; Wu et al, 1986). The following relationships were proposed for initial spray angle θ, and initial average drop diameter d:

$$\tan(\theta/2) = \frac{1}{A} 4\pi \left(\frac{\rho_g}{\rho_f} \right)^{1/2} f(T) \qquad (4)$$

$$d = B \frac{2\pi\gamma}{\rho_g V_i^2} x_{max}(T) \qquad (5)$$

where the aerodynamic breakup parameter $T = \rho_f/\rho_g \, (Re/We_f)^2$. The functions f and x_{max} tend to $3^{1/2}/6$ and 3/2, respectively when T is greater than unity. A and B are constants whose values depend on the nozzle geometry and must be determined experimentally. Of note is that the Weber number We_f is based on the fuel properties, injection velocity and on nozzle diameter, not on the gas properties and on fuel droplet size.

The spray angle is essentially linearly proportional to the square root of gas density, being independent of injection velocity if the function f is constant. This relation for spray angle was confirmed by extensive experiments

by Reitz and Bracco(1982). In the current experimental results, the Reynolds numbers are 700 at 20 m/s and 1400 at 40 m/s. The values of the aerodynamic breakup parameter T are 2 at 20 m/s, and 0.5 at 40 m/s when p_c = 300 psig. Since the density of nitrogen at 600 psig is 1.95 times larger than at 300 psig, those at 600 psig are about one half of those at 300 psig, being 1 and 0.25, respectively. The values of the function f from Reitz and Bracco(1982) were calculated to be 0.21 at V_j = 20 m/s and 0.18 at V_j = 40 m/s when p_c = 300 psig; and 0.20 at V_j = 20 m/s, and 0.18 at V_j = 40 m/s when p_c = 600 psig. The values of the geometrical parameter A for the electrostatic spray triode were calculated to be 2.02, 1.99, 1.96 and 2.05 with an average of 2. The current data support that the spray angle of the fuel jet can be predicted if the geometrical parameter A is known for a particular nozzle.

The average droplet size from Eq. (5) is inversely proportional to the square of the injection velocity and to the density of gas which the fuel is injected into, if x_{max} is constant. Although the detailed sizes of droplets were not measured at E = 0 kV, Fig. 10 clearly shows that the droplet size becomes much smaller if the injection velocity is doubled at the same pressure. However, when the injection velocity is the same, the droplets tend to increase in size with increase in gas density or pressure which is opposite to Eq. (5). A recent experimental study by Wu et al. (1986) reported similar behavior. Drop coalescence leads to a rapid increase in drop size, particularly at high gas density, which may be prevented by electrostatic repulsion.

With Electric Charge

When fuel was injected into air at 0 psig (atmospheric pressure) a single stream of fuel was observed all the way across the window without electric charge

even at the flow injection velocity of 40 m/s (Fig. 10a). However, the fuel jet breaks up when the voltage is applied, not shown since similar photos were shown in an earlier paper (Bankston et al, 1988). As the charge density increased, the break up of fluid occurred earlier, and the spray angle increased more rapidly. It seems that the droplet size becomes smaller as the charge density increases.

At p_c = 300 psig, and V_i = 20 m/s the fuel jet breaks up without the applied voltage (Fig. 10b). However, the applied voltage caused the fuel stream to break up considerably more and increases the initial spray angle to almost 180^0 at E = -12kV (Fig. 11a). A large number of small droplets were observed everywhere except in the dense core which extended to about 1.5 cm beyond the nozzle at E = -10kV(Fig. 11b). At E = -12kV, there was significant fuel jet breakup in the near proximity of the orifice, and large lateral dispersion of the charged droplets. If soot is primarily formed in the fuel rich region such as a dense core region, electrostatic dispersion should reduce the formation of soot. Similar behavior was observed for the higher injection velocity V_i = 40 m/s. Since the inertia force is larger, however, the dense core region extended to 3 cm at E = -10kV (Fig. 11c) and to 2.5 cm at E = -12kV (Fig. 11d).

The drop size distributions were obtained using image processing for Figs. 11a, 11b and 11d. Details on the procedure are given in the Appendix. The drops in the three areas in Fig. 11b were examined. About 20 drops in each region were processed and the average diameters, d_{10}, were estimated to be 235, 235 and 240 μ, respectively. Since the drop size distributions in the three regions are similar, the values of d_{10} and d_{32} for all drops in the three regions were calculated. They are 236 and 242 μ, respectively. The detailed distribution is shown in the bottom of Fig. 12. The average charge density of fuel drops was obtained from Fig. 5 and was plotted in Fig. 13 as a function of the drop

diameter, d_{10}. For comparison, the Rayleigh limit and Kelly's prediction (1982) are included as solid lines. The current averaged value is higher than Kelly's prediction but is lower than the Rayleigh limit. This is the same as the previously reported result (Bankston et al., 1988). The same estimation of drop size was done for one region in Fig. 11a. The drop size distribution is shown in the top of Fig. 12. Even though the charge density is higher than the previous case (Fig. 5), the drop sizes are larger. The values of d_{10} and d_{32} are 367 and 384 μ, respectively. As shown in Fig. 13, the data is close to the Rayleigh limit.

In the case of the higher injection of V_i = 40 m/s (Fig. 11d) the drop size distribution is similar to that of V_i = 20 m/s at E = - 10 kV even though the aerodynamic force on the fuel jet is four times larger. The values of d_{10} and d_{32} are 234 and 241 μ, respectively (sample size, N_{Total} = 85). The charge density was about 0.9 C/m^3 which is the same order of that of V_i = 20 m/s at E = -10 kV (ρ_e = 0.78 C/m^3). Therefore, it seems that the drop size is determined by the charge density rather than by the aerodynamic forces. Since high injection of fuel tends to increase the fuel rich or dense core region, better performance is expected at the lower injection velocities. However, the performan of electrostatic dispersion should be optimized by adjusting various parameters such as the injection velocity, electric potential and nozzle size to inject a certain amount of fuel in an engine to produce a suitable size of drops and less fuel rich or dense core regions. A flow visualization study was attempted for the higher back pressure of 600 psig, but it was not successful due to the failure of the insulation in the electrostatic spray triode.

Summary and Conclusions

The results of this investigation are summarized as follows:

1. Charge density measurements (p_c = 0 psig)
   i. The total charge emitted by the cathode per unit time increased linearly with the electric potential until breakdown occurred. After breakdown occurred, the total current sharply increased by 5 to 10 times depending on flow rates and again gradually increased as the electric potential increased.
   ii. The charge swept downstream by the fuel showed a similar behavior as the total charge, but decreased by 40 to 60 % depending on flow rate when breakdown occurred.
   iii. The ratio of the charge swept downstream to the total emitted charge was 0.1 to 0.4 before breakdown and was smaller than 0.05 after breakdown.
   iv. As the flow rate increased, breakdown occurred at higher voltages; -8.5 kV at 0.51 mℓ/s to -13 kV at 2.5 mℓ/s.
   v. The maximum charge density increased with flow rate ,reached a maximum value of 1.65 C/m^3, remained at the maximum value for a range of flow rates and decreased slightly with further increase of flow rate.
2. Charge density measurements (p_c = 300 and 600 psig)
   i. The charge density at high back pressures exhibited similar behavior as those at p_c = 0 psig; the charge density increased with electric potential at a fixed flow rate and decreased with flow rate at a fixed applied voltage.

ii. The charge density decreased with increasing back pressure before breakdown occurred; being smaller than that at 0 psig by 10-17 % for 300 psig and by 40-50 % for 600 psig when $\dot{Q}$ = 0.51 mℓ/s.

iii. The maximum charge density was also smaller by 20-26 % for 300 psig and by 22-43 % for 600 psig depending on flow rate when the applied voltage was limited below -14 kV.

iv. Breakdown occurred at a higher voltage as the back pressure increased; at -8.5 kV for p_c = 0 psig, at -10 kV for p_c = 300 psig and at -11 kV for p_c = 600 psig when $\dot{Q}$ = 0.51 mℓ/s.

v. The decrease in the charge density right after breakdown was much smaller at higher back pressures; 20 % reduction for 300 and 600 psig, compared to 50 % for 0 psig at $\dot{Q}$ = 0.51 mℓ/s.

3. Flow Visualization

i. In general, with electric charge, rapid breakup of the jet was achieved without large droplets in the core region.

ii. The spray angle increased to larger than 180^{o} with increase of electric potental which enhanced dispersion of fuel near the nozzle exit and reduced the dense core region.

iii. It was observed that the size of drops may be determined by the charge density rather than by aerodynamic forces.

The present investigation has indicated significant early breakup and dispersion of charged diesel fuel jets by using an electrostatic spray triode at high back pressures compared to aerodynamic breakup and dispersion. These results are encouraging for engine injection, but demonstration of this technique under pulsed fuel injection and autoignition conditions requires subsequent investigations to evaluate the potential for improvement in combustion and reduced soot formation.

Acknowledgments

This paper describes the results of research carried out by the Jet Propulsion Laboratory, California Institute of Technology and was supported by the U. S. Army Research Office through an agreement with the National Aeronautics and Space Administration. The authors express their appreciation to Messrs. J. J. Godley and S. Kikkert for their contributions in fabrication and assembly of the test setup, and in the conduct of the experiments. They also express their appreciation to Dr. Kenneth Harstad for his assistance in the analysis of droplet sizes and to Dr. Parthasarathy Shakkottai for discussions on charge transport. The Spray Triode is used by permission of Mr. Harold Simmons of the Parker Hannifin Corporation.

References

Ahmad, T., Speck, C. E., and Sing, D. C., (1980), "Effect of Electric Fields Applied Within the Prechamber on Particulate Emissions from a Diesel Engine," presented at the Fall Technical Meeting, Western States Section, Combustion Institute, General Motors Research Report No. GMR-3326, October.

Bankston, C. P., Back, L. H., Kwack, E. Y., and Kelly, A. J., (1988), "Experimental Investigation of Electrostatic Dispersion and Combustion of Diesel Fuel Jets," ASME J. Engr. Gas Turbines and Power, Vol. 110, No. 3, pp. 361-368.

Bellan, J., (1983), "A New Approach to Soot Control in Diesel Engines by Fuel Drop Charging," Combustion and Flame, Vol. 51, pp. 117-119.

Bellan, J. and Cuffel, R., (1983), "A Theory of Nondilute Spray Evaporation Based upon Multiple Drop Interactions," Combustion and Flame, Vol. 51, pp. 55-67.

Bellan, J. and Harstad, K., (1987), "Details of the Convective Evaporation of Dense and Dilute Clusters of Drops," Int. J. Heat Mass Transfer, Vol. 30, No. 6, pp. 1082-1093.

Bellan J. and Harstad, K., (1988), "Turbulence Effects During Evaporation of Drops in Clusters," to be published in Int. Heat Mass Transfer.

Gaffney, J., Sapieza, R., Butcher, T., Drishna, C., Marlow, W., and O'Hare, T., (1980), "Soot Reduction in Diesel Engines: A Chemical Approach," Combustion Science and Technology, Vol. 24, pp. 89-92.

Harstad, K. G. and Bellan, J., (1988), "Electrostatic Dispersion of Drops in Clusters," to be published.

Inuishi, Y., (1979), "High Field Conduction and Breakdown in Dielectric Liquids," J. Electrostatics, Vol. 7, pp. 1-12.

Kelly, A. J., (1981), "Electrostatic Atomizing Device," U. S. Patent No. 4,255,777, March 10.

Kelly, A. J., (1982), "The Electrostatic Atomization of Hydrocarbons," Proceedings of the 2nd Int. Conf. on Liquid Atomization and Spray Systems, June.

Khan, I. M., Wang, C. H. T., and Langridge, B. E., (1972), "Effect of Air Swirl on Smoke and Gaseous Emissions from Direct-Injection Diesel Engines," SAE paper No. 720102.

Lin, S. P. and Kang, B. J., (1987), "Atomization of a Liquid Jet," Physics of Fluids, Vol. 30, No.7. pp. 2000-2006.

Luther, F. E., (1962), "Electrostatic Atomization of No. 2 Heating Oil," Proc. 2nd API Research Conference on Distillate Fuel Combustion, API Publication No. 1701, June.

Miller, J. A., Biblarz, O, Zajdman, A., Manning, W. W., II, and Mavroudis, J. A., (1987), "Electrostatic Spray Modification in Gas Turbulent Combustion," J. Propulsion and Power, Vol. 3, No. 2, pp. 187-192.

Newgard, P. M. and Noon, A. W., (1964), "Electrostatic Atomizer and Burner Research," Distillate Fuel Combustion Conference, API Publication No. 1725, November.

Pischinger, R. and Cartellieri, W., (1972), "Combustion System Parameters and Their Effect Upon Diesel Engine Exhaust Emissions," SAE paper No. 720765.

Prado, G. P., Lee, M. L., Hites, R. A., Hoult, D. P. and Howard, J. B., (1977), "Soot and Hydrocarbon Formation in a Turbulent Diffusion Flame," Proc. 16th Symp. (Int.) on Combustion, pp. 649-661.

Ranz, W. E., (1958), Can. J. Chem. Eng., Vol. 36, p. 175.

Reitz, R. D. and Bracco, F. V., (1982), "Mechanism of Atomization of a Liquid Jet," Physics of Fluids, Vol. 25, No. 10, pp. 1730-1742.

True, M. A., (1983), "Modeling of Electrostatic Spray Plumes," IEEE/IAS Annual Meeting 1980; IAS Transactions, pp. 993-997.

Wu, k-J., Reitz, R. D., and Bracco, F. V., (1986), "Measurements of Drop Size at the Spray Edge Near the Nozzle in Atomizing Liquid Jets," Physics of Fluids, Vol. 29, No. 4, pp.941-951.

Nomenclature

A	geometrical constant in Eq. (5)
B	geometrical constant in Eq. (6)
d	drop diameter, m
d_n	spray nozzle diameter, m
d_{10}	arithmetic mean diameter, m
d_{32}	volume-surface mean diameter, m
E	electric potential across cathode and anode electrodes, V
f	function in Eq. (4)
i_a	charge attracted to anode per unit time, amp
i_f	charge swept downstream by fuel per unit time, amp
i_t	total charge emitted by cathode per unit time, amp
m_f	fuel mass, g
N	number of fuel drops
p_c	chamber pressure, psig
$\dot{Q}$	fuel flow rate, mℓ/s
Re	Reynolds number, $\rho_f V_j d_n/\mu_f$
T	aerodynamic breakup parameter
V_j	fuel injection velocity, m/s
We_f	Weber number based on fuel properties, $\rho_f V_j^2 d_n/\gamma$
x_{max}	function in Eq. (5)
x_l	length of intact core, m
γ	surface tension of fuel, N/m
ϵ_0	permittivity of free space, 8.85×10^{-12} C/V-m
θ	spray angle, degree

μ_f viscosity of fuel, kg/m-s

ρ_e charge density, C/m^3

$\rho_{e,max}$ maximum charge density, C/m^3

ρ_f fuel density, g/cm^3

ρ_g gas density, g/cm^3

Appendix

Image Processing

Drop sizes were determined in the following manner. Image frames with 512 x 480 pixel resolution were formed over areas approximately 2 cm on a side from a spray photograph. The corresponding pixel size (image physical resolution) is about 45 μm. Any drops of about this size or smaller would not register in the image; at most, they would add an apparent "noise" to the image. Thus measurements were valid down to drop sizes of order 100 μm. Using a mouse guided cursor, isolated, distinct drops in a frame were selected. Pixel values along two perpendicular lines through a drop center were obtained. The first and second moments of these pixel arrays were used to determine an average pixel threshold value corresponding to the RMS drop extension in each direction. The image in a box of pixels surrounding the drop was thresholded and a pixel count of the drop in the threshold image made. Assuming a Gaussian pixel gray level distribution for a drop, the actual drop cross-sectional area is calculated as twice this pixel count.

List of Figures

1. Schematic diagram of experimental setup

2. Currents vs electric potential at p_C = 0 psig and $\dot{Q}$ = 1.2 mℓ/s

3. Charge swept downstream by fuel per unit time vs electric potential for various flow rates at p_C = 0 psig

4. Charge density vs electric potential for various flow rates at p_C = 0 psig

5. Charge density vs electric potential for various flow rates at p_C = 300 psig

6. Charge density vs electric potential for various flow rates at p_C = 600 psig

7. Charge density vs flow rate for various back pressures at E = -8 kV

8. Maximum charge density vs flow rate at back pressures of 0, 300 and 600 psig and at E = -14 kV

9. Maximum charge density vs flow rate at back pressures of 0 and 300 psig and at E = -18 kV

10a. Diesel fuel jet spray at E = 0 kV, V_j = 40 m/s and p_C = 0 psig

10b. Diesel fuel jet spray at E = 0 kV, V_j = 20 m/s and p_C = 300 psig

10c. Diesel fuel jet spray at E = 0 kV, V_j = 40 m/s and p_C = 300 psig

10d. Diesel fuel jet spray at E = 0 kV, V_j = 20 m/s and p_C = 600 psig

10e. Diesel fuel jet spray at E = 0 kV, V_j = 40 m/s and p_C = 600 psig

11a. Diesel fuel jet spray at E = -12 kV, V_j = 20 m/s and p_C = 300 psig

11b. Diesel fuel jet spray at E = -10 kV, V_j = 20 m/s and p_C = 300 psig

11c. Diesel fuel jet spray at E = -10 kV, V_j = 40 m/s and p_C = 300 psig

11d. Diesel fuel jet spray at E = -12 kV, V_j = 40 m/s and p_C = 300 psig

12. Droplet size distributions of fuel sprays of Figs. 11a and 11b

13. Charge density vs droplet size

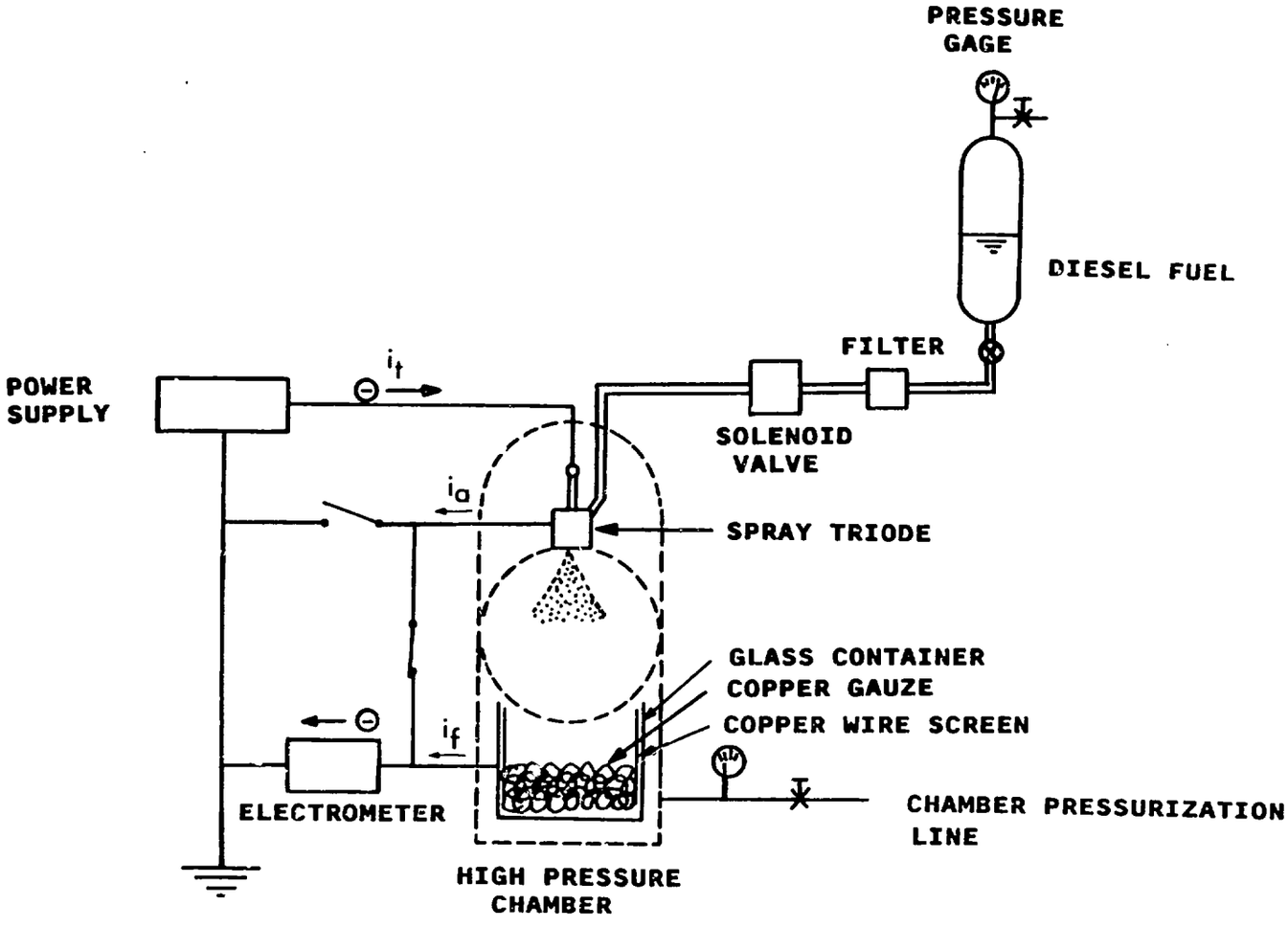
PRESSURE
GAGE
DIESEL FUEL
FILTER
POWER
SUPPLY
i_t
SOLENOID
VALVE
i_a
SPRAY TRIODE
GLASS CONTAINER
COPPER GAUZE
COPPER WIRE SCREEN
i_f
ELECTROMETER
CHAMBER PRESSURIZATION
LINE
HIGH PRESSURE
CHAMBER

Figure 1.

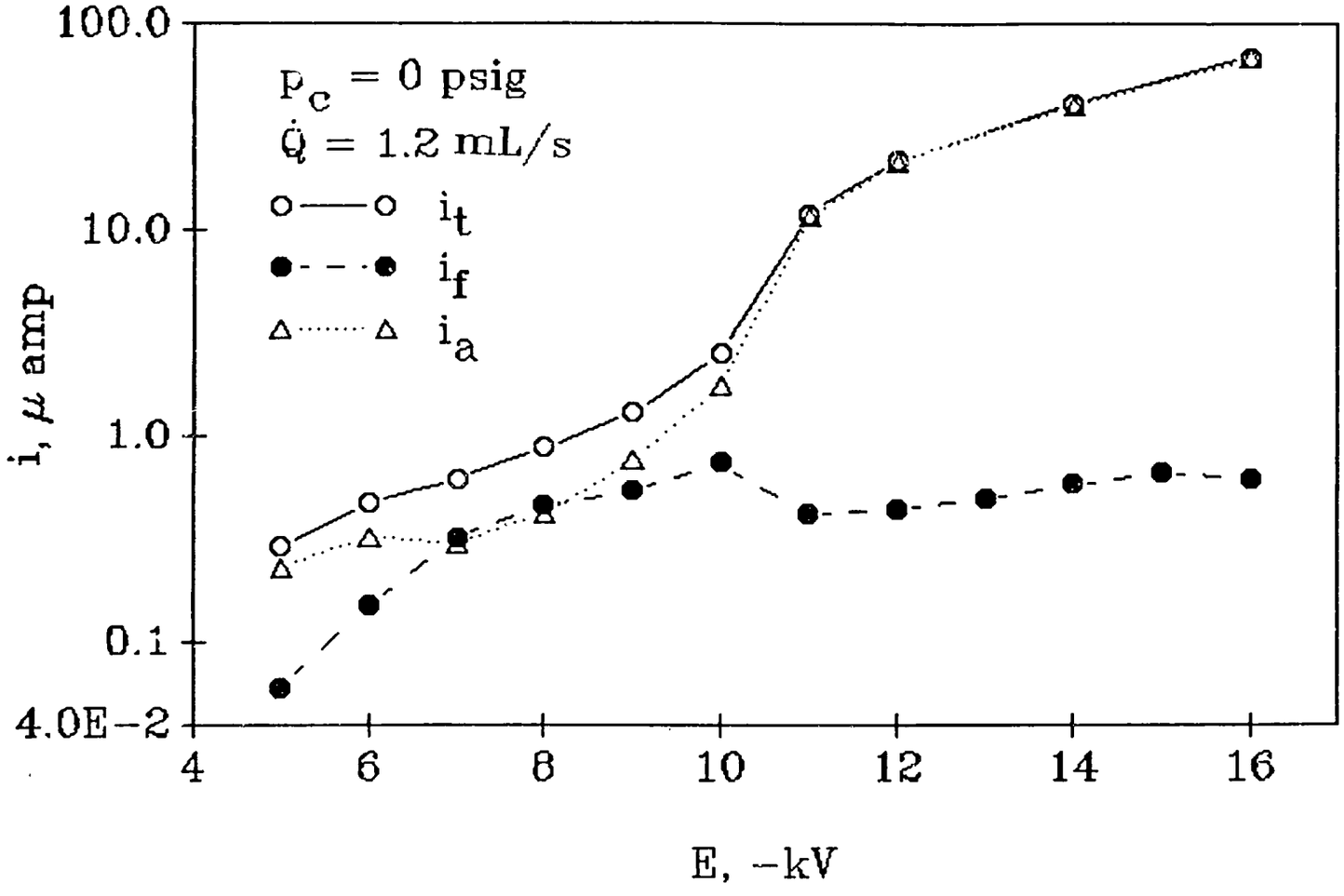
100.0
10.0
1.0
0.1
4.0E−2
p_c = 0 psig
$\dot{Q}$ = 1.2 mL/s
i_t
i_f
i_a
i, μ amp
4
6
8
10
12
14
16
E, −kV

Figure 2.

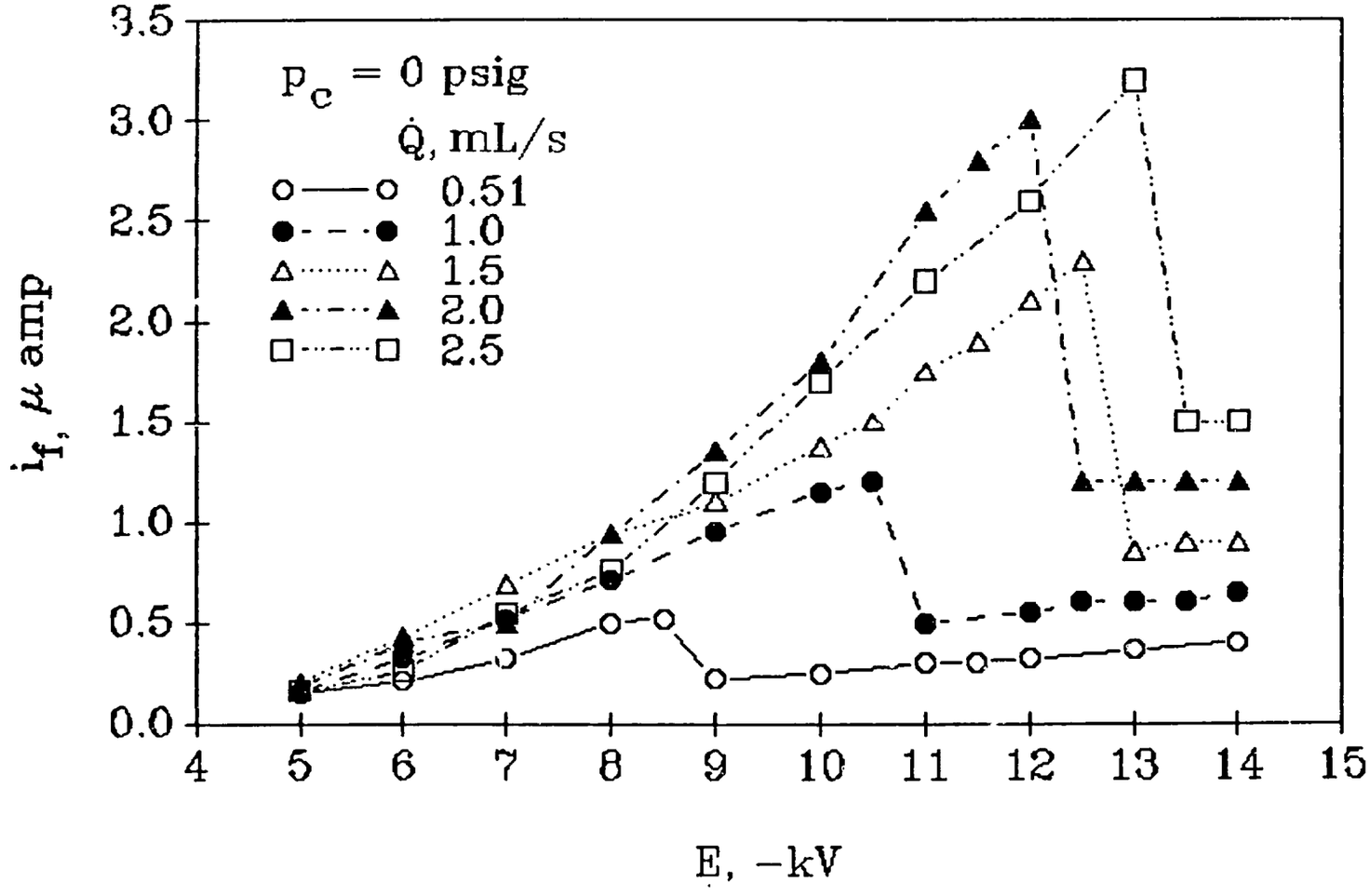
p_c = 0 psig
Q, mL/s
0.51
1.0
1.5
2.0
2.5
i_f, μ amp
E, −kV
0.0
0.5
1.0
1.5
2.0
2.5
3.0
3.5
4
5
6
7
8
9
10
11
12
13
14
15

Figure 3.

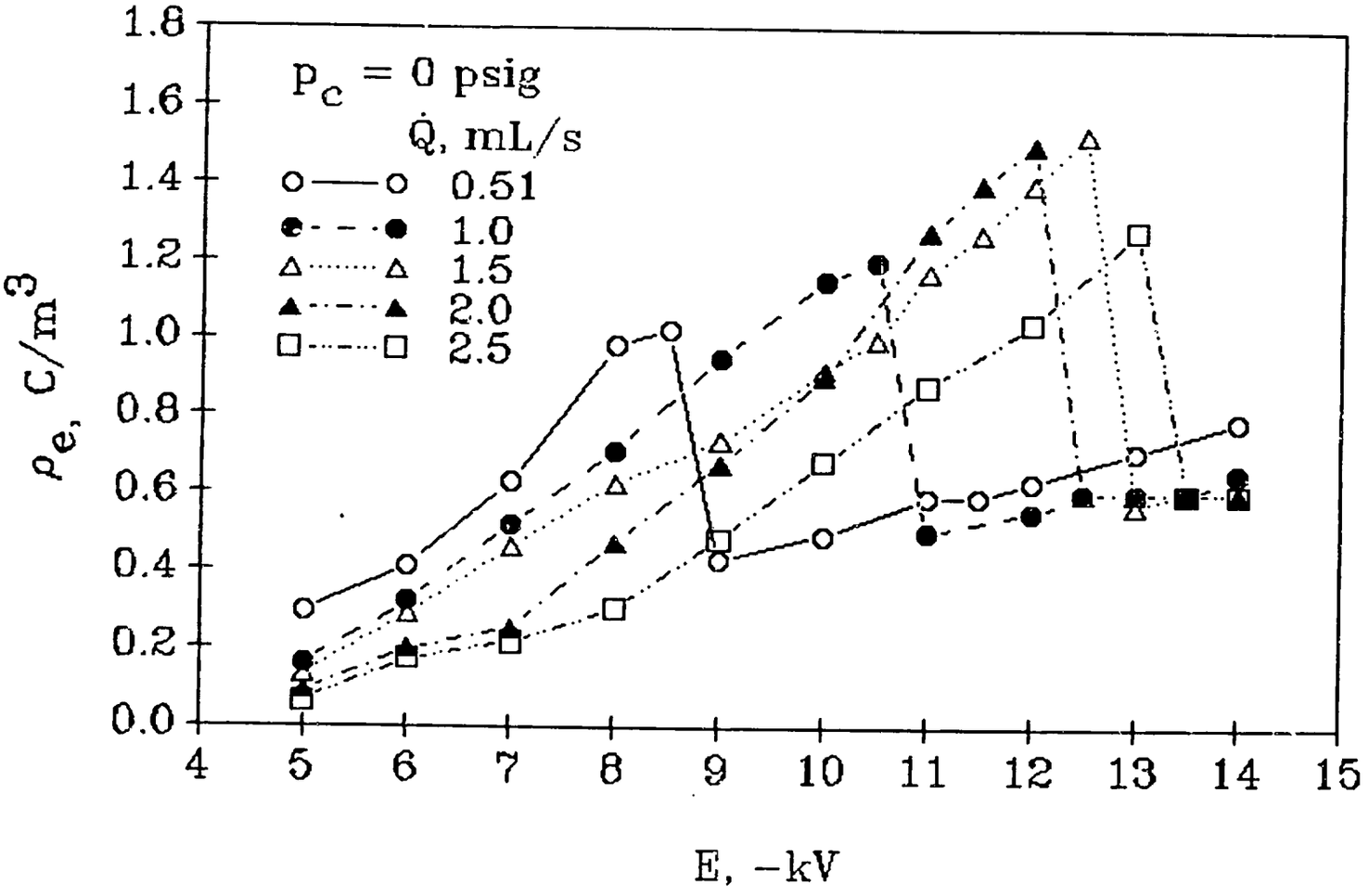
p_c = 0 psig
Q̇, mL/s
0.51
1.0
1.5
2.0
2.5
ρ_e, C/m^3
E, −kV
1.8
1.6
1.4
1.2
1.0
0.8
0.6
0.4
0.2
0.0
4
5
6
7
8
9
10
11
12
13
14
15

Figure 4.

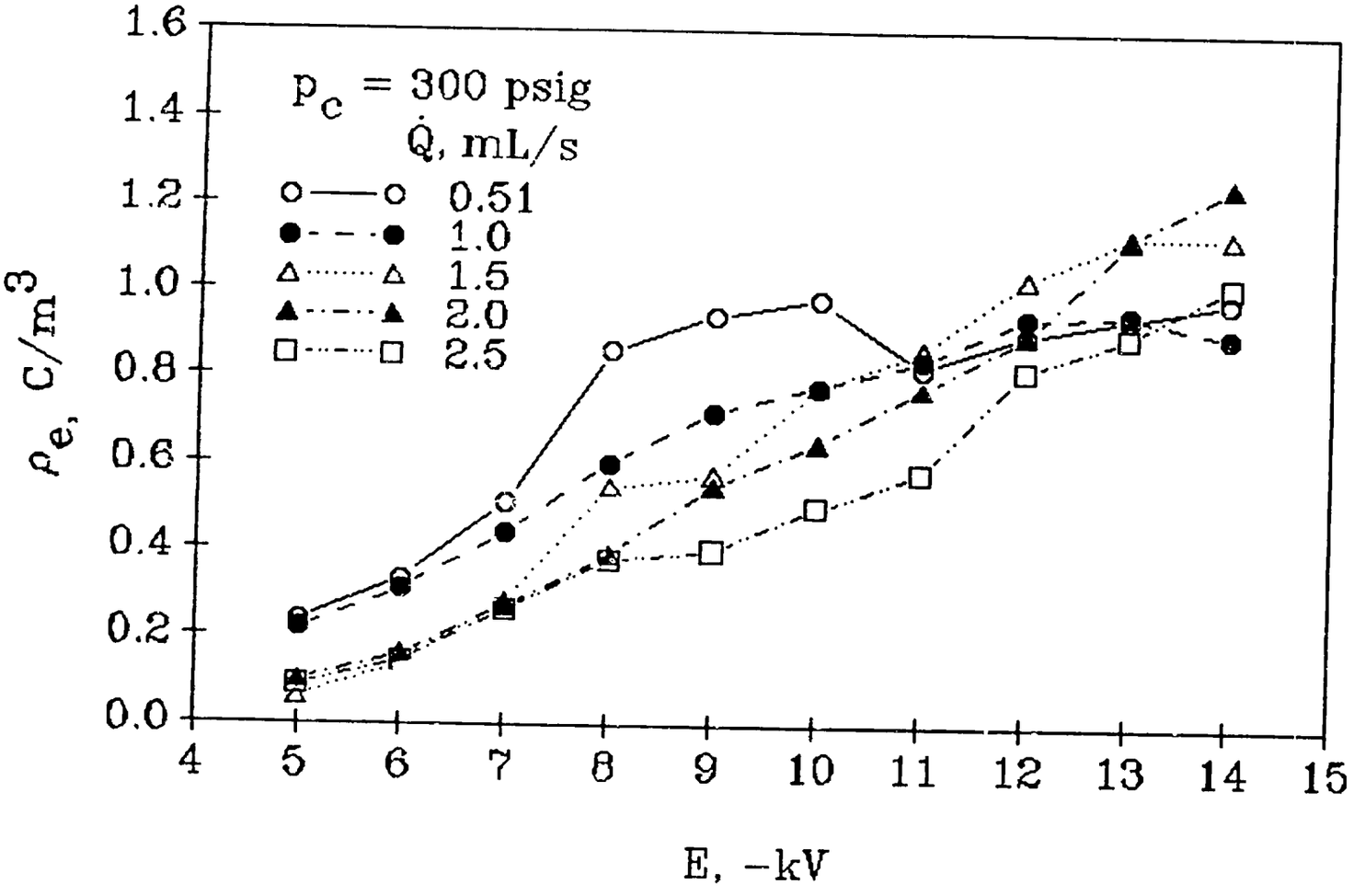
p_c = 300 psig
Q̇, mL/s
0.51
1.0
1.5
2.0
2.5
ρ_e, C/m^3
E, −kV
1.6
1.4
1.2
1.0
0.8
0.6
0.4
0.2
0.0
4
5
6
7
8
9
10
11
12
13
14
15

Figure 5.

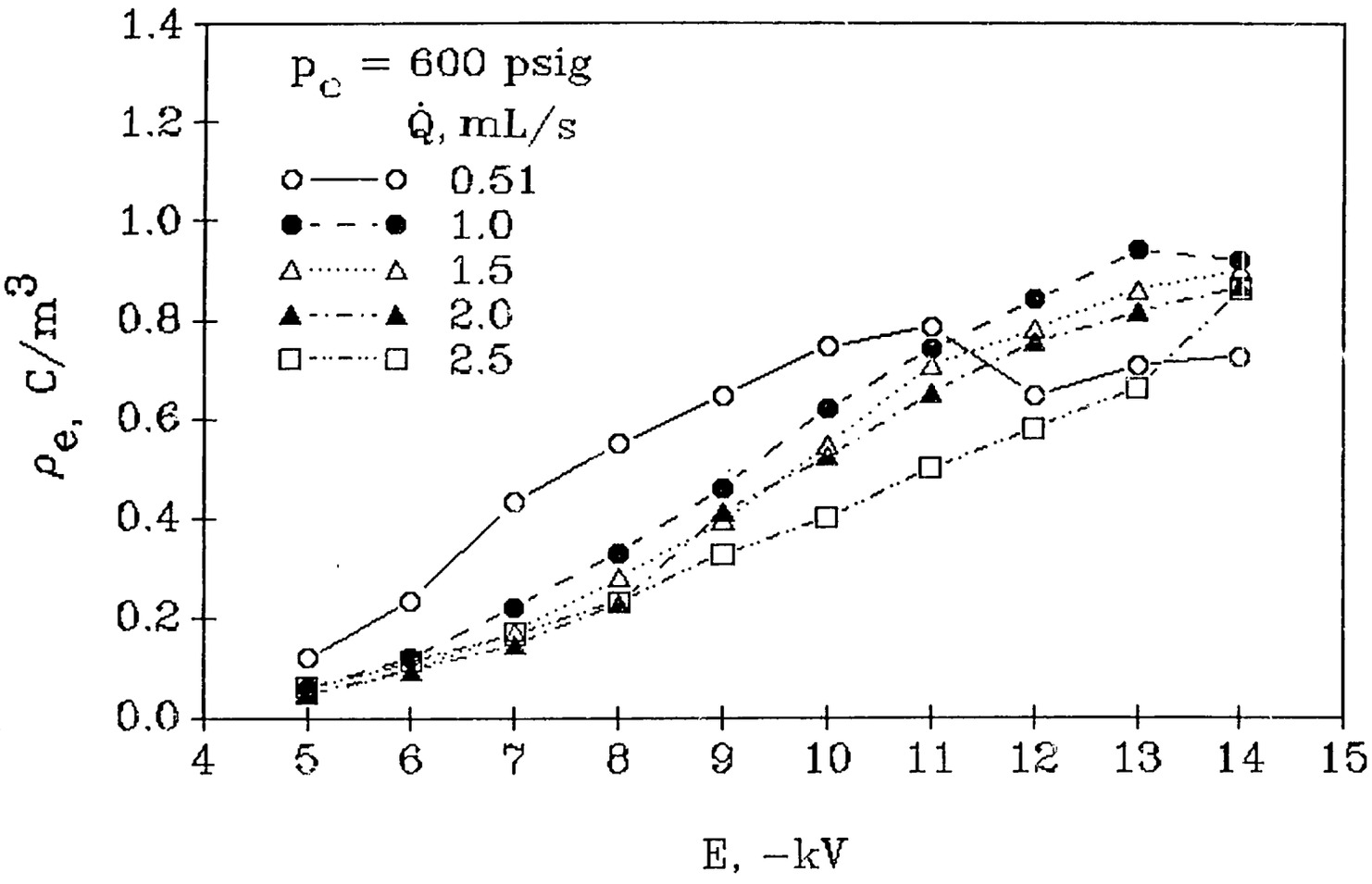
p_c = 600 psig
Q̇, mL/s
0.51
1.0
1.5
2.0
2.5
ρ_e, C/m^3
E, −kV
1.4
1.2
1.0
0.8
0.6
0.4
0.2
0.0
4
5
6
7
8
9
10
11
12
13
14
15

Figure 6.

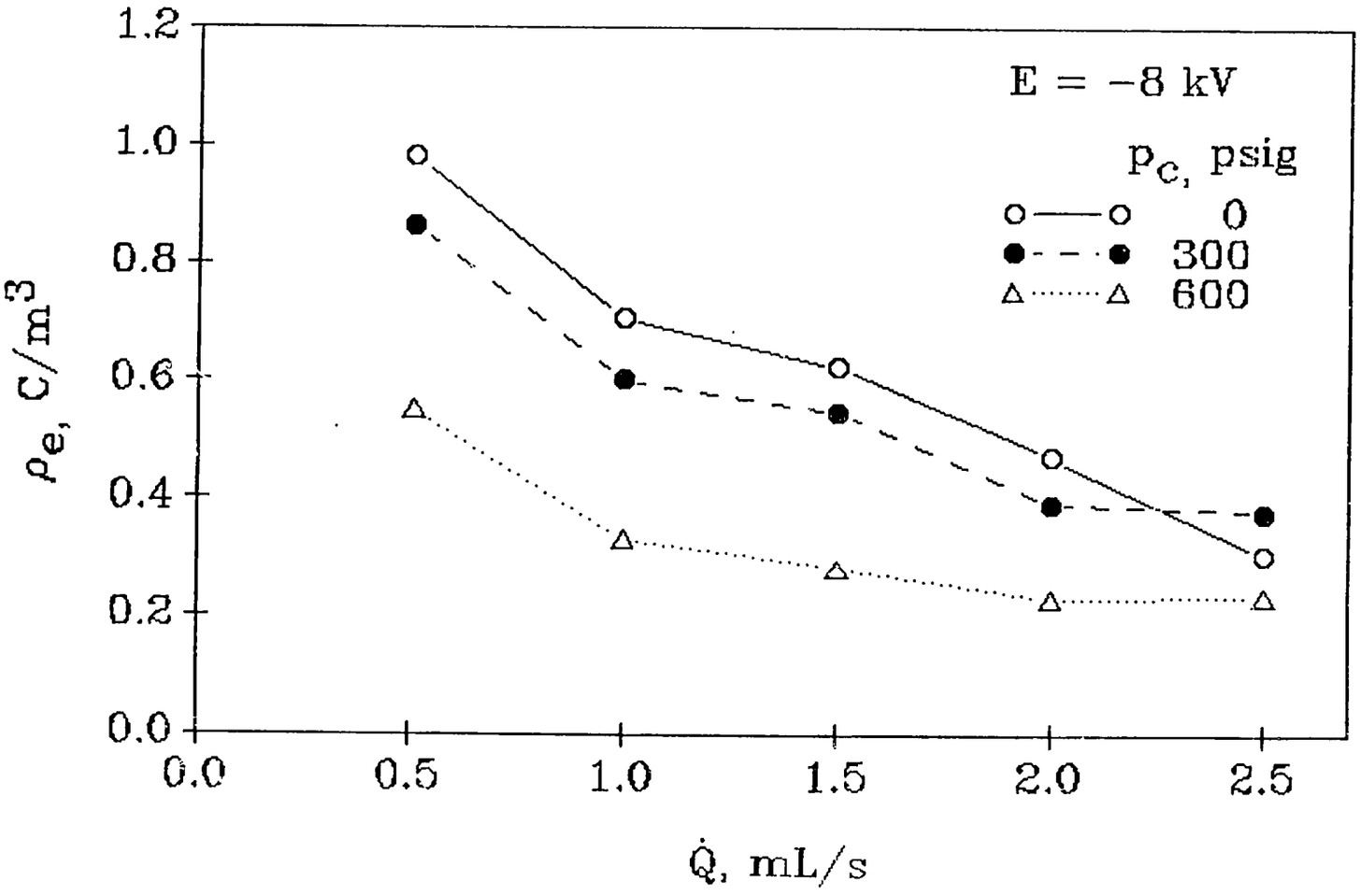
E = −8 kV
p_c, psig
0
300
600
ρ_e, C/m^3
1.2
1.0
0.8
0.6
0.4
0.2
0.0
0.0
0.5
1.0
1.5
2.0
2.5
$\dot{Q}$, mL/s

Figure 7.

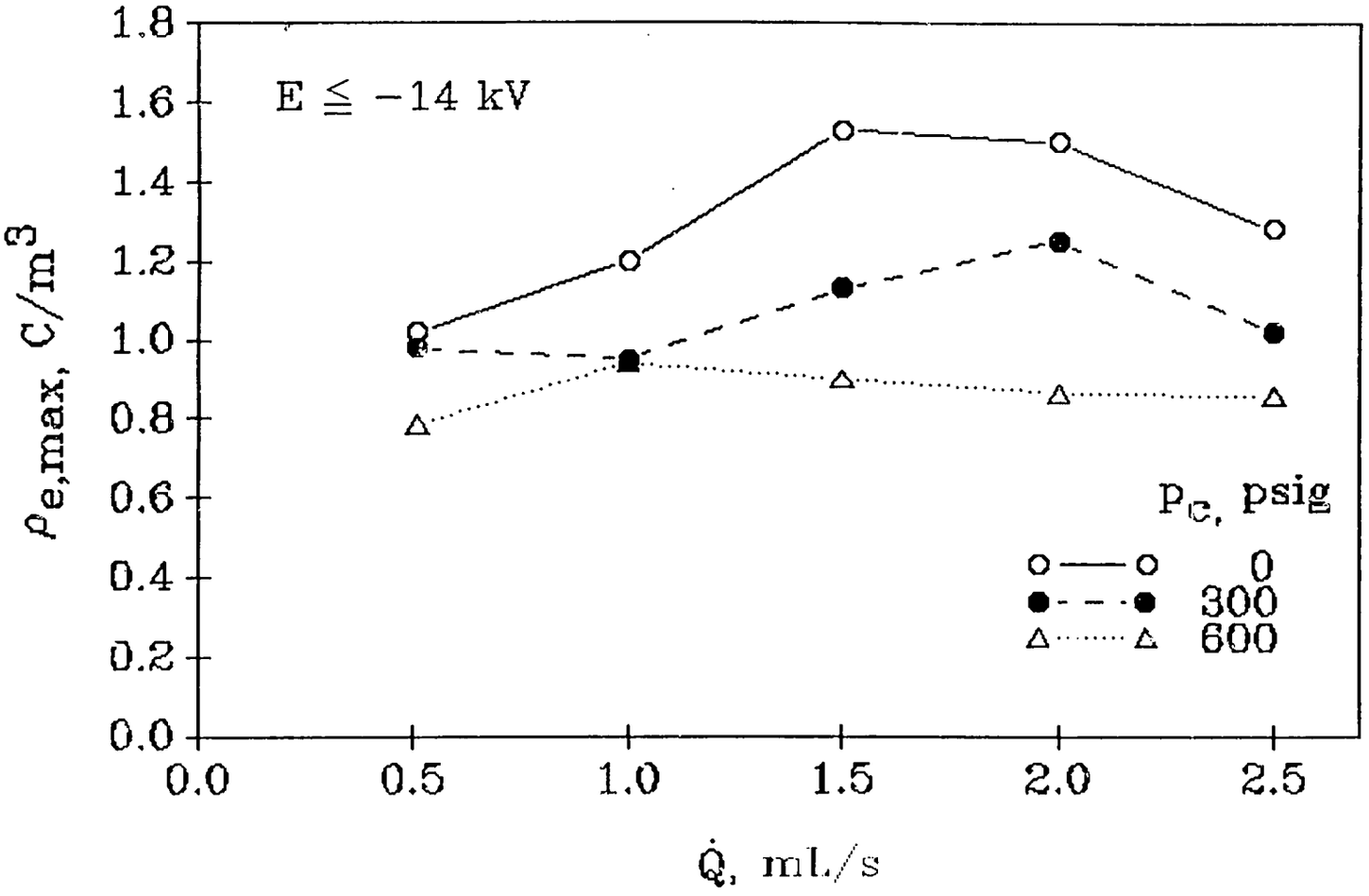
E ≦ −14 kV
$\rho_{e,max}$, C/m^3
1.8
1.6
1.4
1.2
1.0
0.8
0.6
0.4
0.2
0.0
0.0
0.5
1.0
1.5
2.0
2.5
$\dot{Q}$, mL/s
P_C, psig
0
300
600

Figure 8.

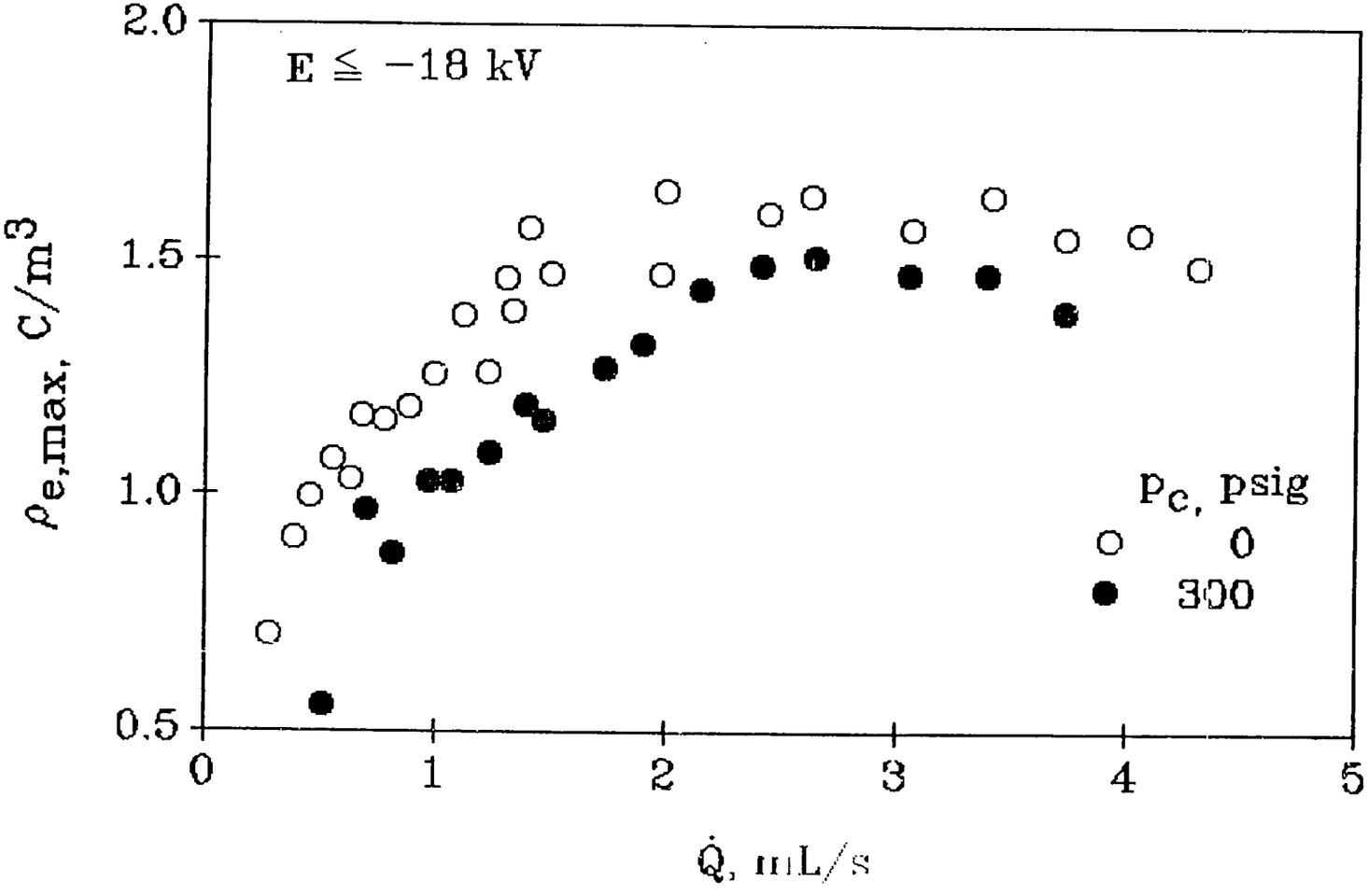

Figure 9.

Figure 10a.

Figure 10b.

Figure 10c.

Figure 10d.

Figure 10e.

Figure 11a.

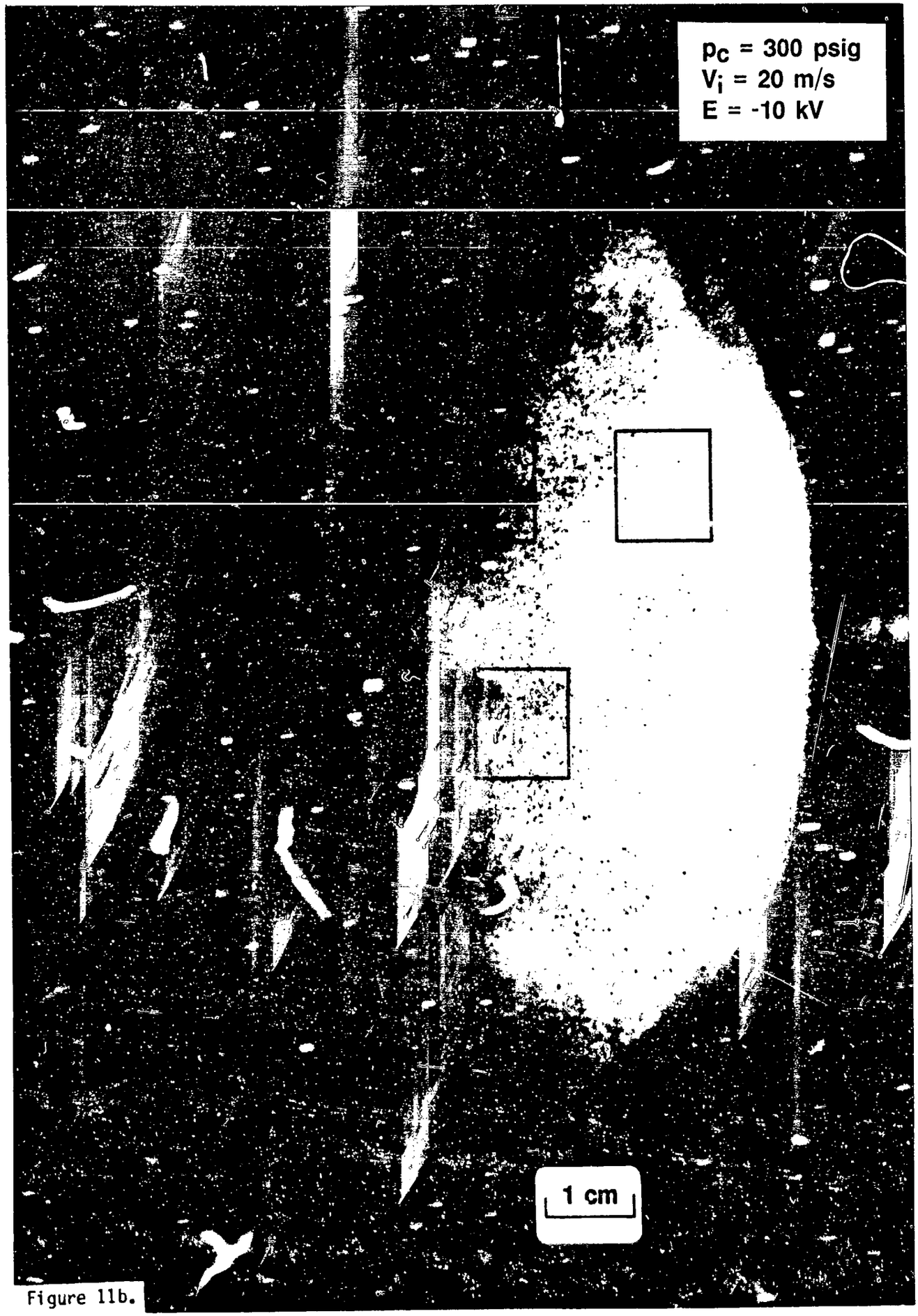

Figure 11b.

Figure 11c.

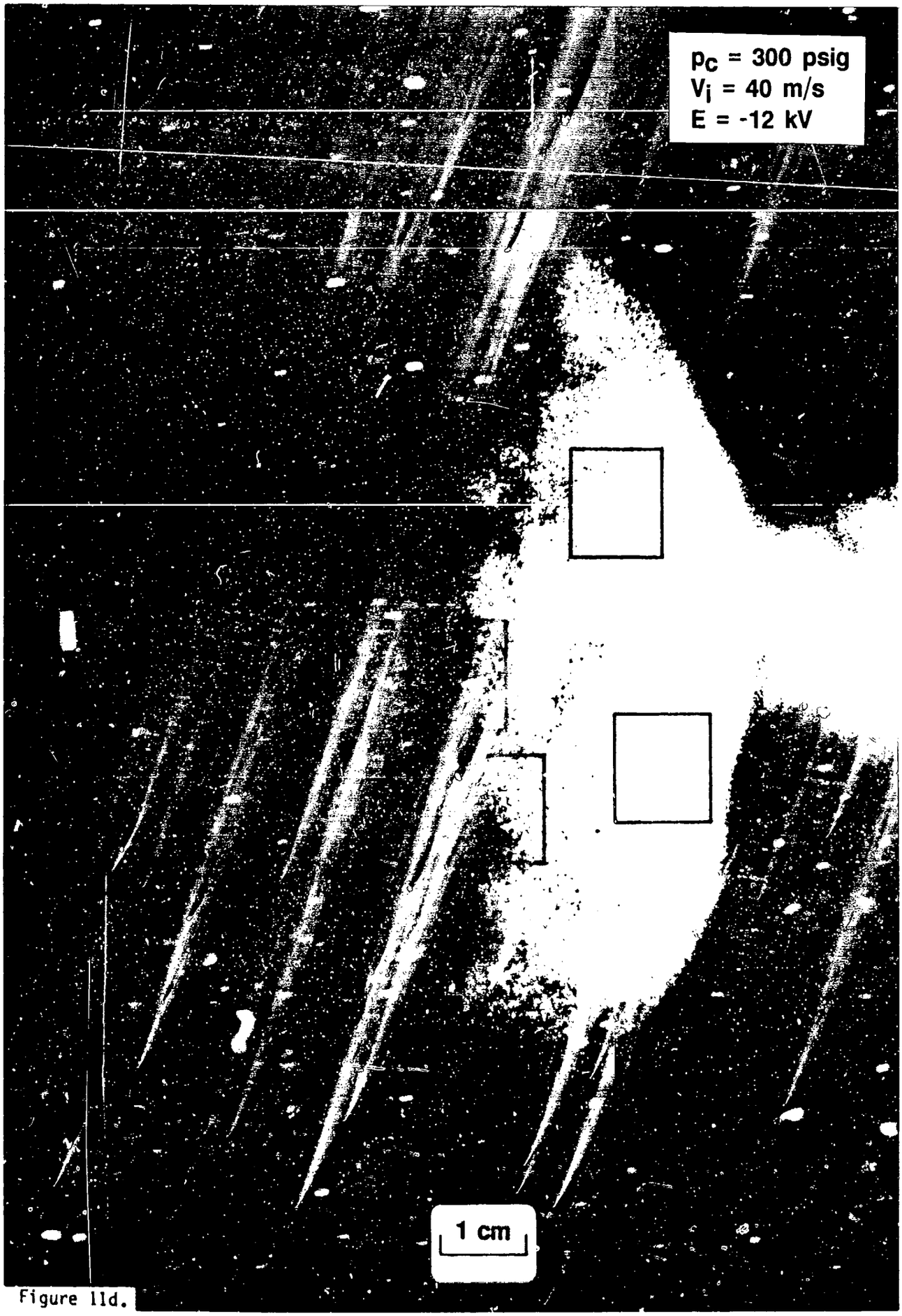

Figure 11d.

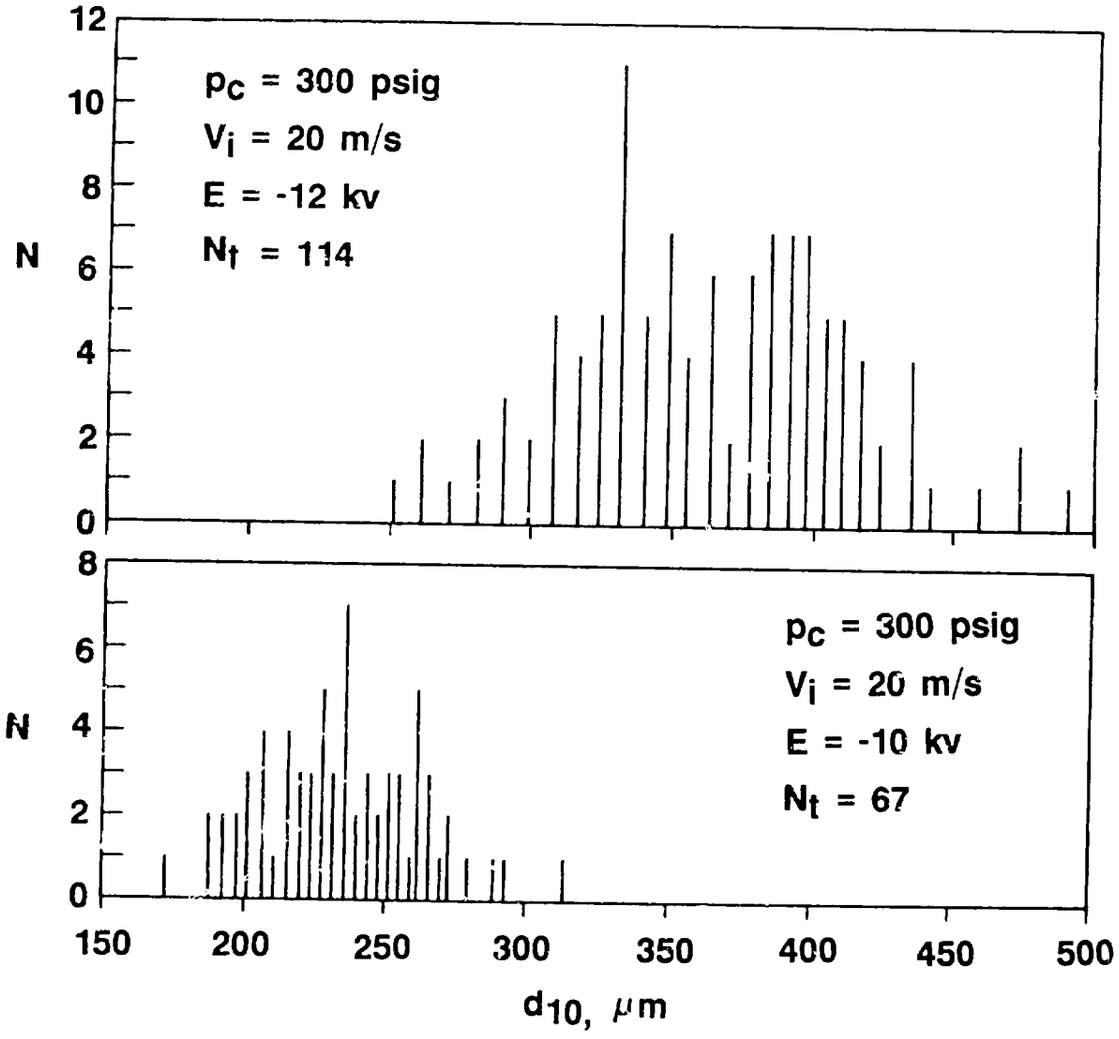
12
10
8
6
4
2
0
N
p_c = 300 psig
V_i = 20 m/s
E = -12 kv
N_t = 114
8
6
4
2
0
N
p_c = 300 psig
V_i = 20 m/s
E = -10 kv
N_t = 67
150
200
250
300
350
400
450
500
d_{10}, μm

Figure 12.

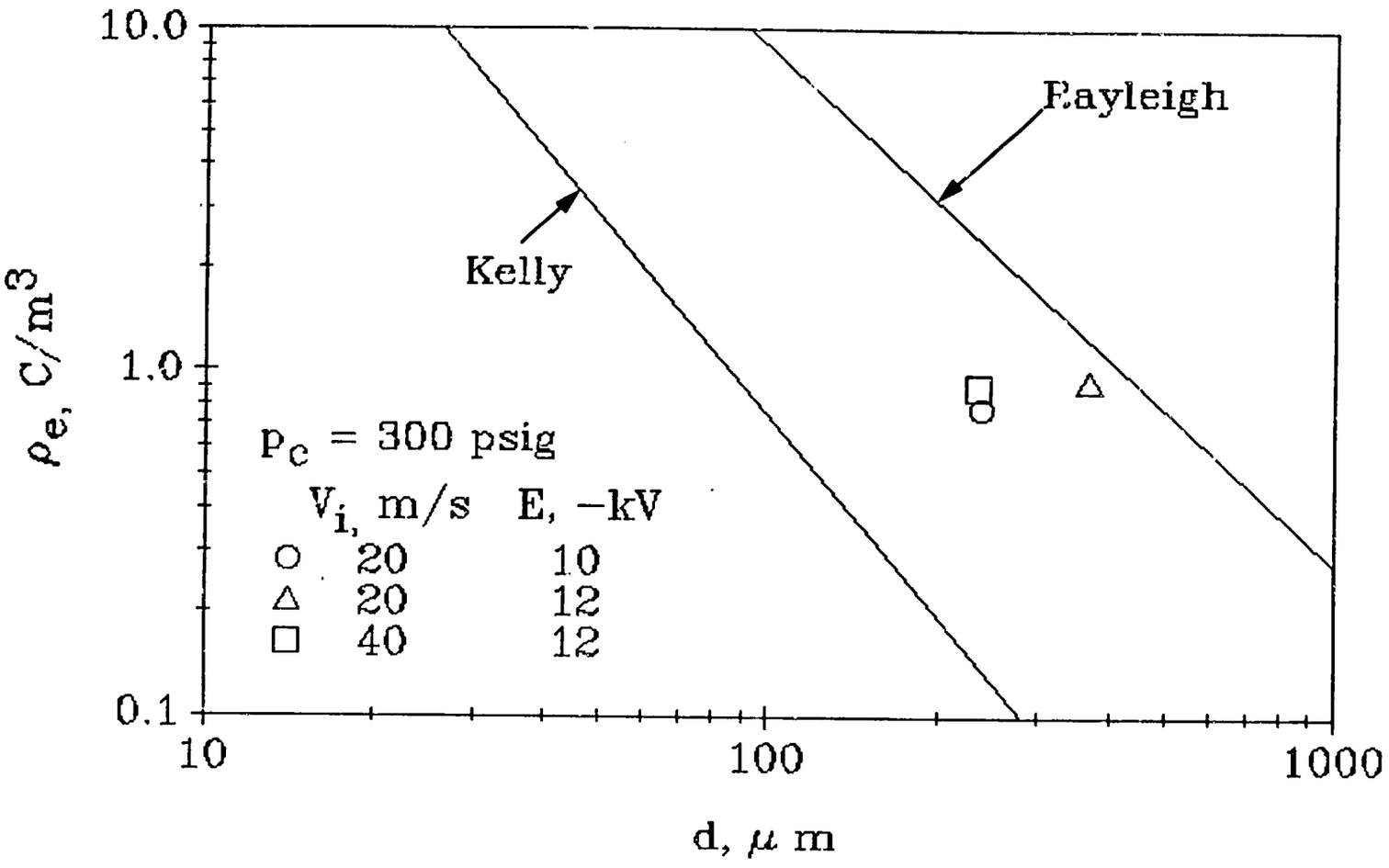
10.0
1.0
0.1
10
100
1000
ρ_e, C/m^3
d, μ m
Rayleigh
Kelly
p_c = 300 psig
V_i, m/s E, −kV
○ 20 10
△ 20 12
□ 40 12

Figure 13.

Appendix II

ELECTROSTATIC DISPERSION OF DROPS IN CLUSTERS

K. Harstad and J. Bellan

Jet Propulsion Laboratory
California Institute of Technology
Pasadena, CA 91109

Abstract

A theory of evaporation and dispersion of electrostatically charged drops has been developed for drops belonging to a spherical cluster exposed to a flow. Under the assumption of constant atmospheric pressure, the quasi-steady approximation was made for the gas phase whereas the drop-temperature history is unsteady. The model takes into account interdrop interactions (in terms of heat and mass transfer) due to drop proximity, turbulence exchange processes between the cluster and its surroundings and electrostatic force effects due to the charge on the drops. Calculations based upon this model were made for charged as well as uncharged clusters of drops. The charge was varied from a null value to the maximum possible charge found empirically for hydrocarbon sprays. Moreover, the turbulence model was varied in such a way as to simulate the cluster embedded into a flow where turbulence develops with time (Model 1) or a flow with pre-existing turbulence (Model 2). The results show that the control parameters for the evaporation of charged drops are different from those for uncharged drops in dense clusters; turbulence levels which were shown to be crucial for the latter in the dense cluster regime do not affect the former in the same regime. For dilute clusters turbulence is unimportant in both cases. Moreover, drop charging does not affect dilute clusters of drops whereas dense clusters of drops are substantially affected. Based upon existing experimental data, inferences are made about how electrostatic spray dispersion can affect soot control in power systems using fuel sprays. Limited results pertaining to the ignition of nearly-dense clusters of electrostatically charged drops are discussed as well.

I. Introduction

Power systems using fuel sprays are widely used for mobile and stationary power generation. Unfortunately, one of their important drawbacks is the fact that they produce non-negligible amounts of soot. The soot is formed in the fuel rich regions of the spray through the following process. In general the fuel rich regions of the spray correspond to dense clusters of drops evaporating and producing a large amount of fuel vapor that is not consumed fast enough in the flame. This fuel vapor accumulates without burning and thus instead of being transformed into the usual products of combustion undergoes another set of reactions (pyrolysis reactions) which transform it into soot. Consistent with this observation, mixing and controlled atomization have good potential to reduce soot yield in spray flames (Prado et al., 1977).

Among various means of controlling soot formation, electrostatic charging of the drops was considered promising by Bellan (1983) in the particular case of Diesel engines. Previous investigators (Mayo and Weinberg, 1970; Thong and Weinberg, 1971) had also considered dispersing particles using electric effects, although not specifically for Diesel engines. Mayo and Weinberg (1970) have shown that an applied electric field can reduce both the size and the number rate of formation of soot particles in atmospheric diffusion flames. The situation in Diesel engines was also investigated by Ahmad et al. (1980) and it was shown that, unlike in Mayo and Weinberg (1970), the mass of particulates emitted increased substantially when electric fields were applied. The difference between the results of Mayo and Weinberg (1970) and Ahmad et al. (1980) was attributed to the basic difference of the two combustion systems, but no physical mechanisms accounting for the observations could be provided because there was a lack of study of the fundamental phenomena. In Bellan (1983),

through a very simple calculation, based upon a model of evaporation of dense clusters of drops (Bellan and Cuffel, 1983), it was shown that electrostatic drop charging could be achieved in a Diesel engine and that it would disperse the drops from a dense configuration to dilute configurations where soot formation is no longer a problem. Moreover, the added benefits of secondary atomization induced by charging were also mentioned in Bellan (1983). Roth and Kelly (1983) showed indeed that convulsive disruption occurs during charged-droplet evaporation, yielding a limited number of siblings, about seven. However in Bellan (1983), no definite conclusions could be asserted because the model used was rather restrictive in its assumptions. A simple model of electrostatic spray plumes was also developed by True (1983), but in that model, unlike in Bellan (1983), no account was taken of droplet evaporation or droplet interactions due to their proximity. However, limited drag effects were accounted for by True (1983) unlike the model upon which the work of Bellan (1983) was based (Bellan and Cuffel 1983).

Recent progress in modeling of dense collections of evaporating drops (Bellan and Harstad, 1987a, 1987b) and also new experimental and theoretical results related to electrostatic atomization (Sangiovanni and Liscinsky, 1984) have reopened the question of whether electrostatic spray atomization is a good way to disperse drops and if so in which regimes should it be considered. Additionally, one should know what are its disadvantages, if any.

The present work answers some of these questions and shows that the control parameters for the evaporation of electrostatically charged drops clustered together are different from those of uncharged drops in clusters in the dense cluster regime. The present model pertains to combustion at atmospheric pressure. Instead of performing soot calculations which could be limited by the use of a simple kinetic model, we make inferences regarding the

impact of charging upon soot control in heterogeneous flames by using already existing experimental observations of soot formation in well-defined sprays (Sangiovanni and Liscinsky, 1984). Since this model is expected to yield predictions of qualitative rather than quantitative value, no attempt is made to make detailed comparisons of experiments with the idealized situation considered below. The focus is here on showing that electrostatic spray charging can conceivably be used to disperse drops in a regime that is useful to control soot production.

II. Formulation

Under consideration is a monodisperse, uniformly distributed cluster of drops in a spherical configuration where each drop may be equally charged. The cluster as a whole is assumed to move in a straight line trajectory through an ambient gas at constant pressure, and as it does so, the cluster may undergo radial expansion due to mutual repulsion of the charged drops.

The gas inside the cluster is at the same, constant, pressure as the gas outside the cluster. On a large length scale (many drop diameters), the cluster is taken to be spatially homogeneous in thermodynamic quantities. A coordinate system fixed with the ambient gas is used. In this system, the drops have two velocity components as shown in Figure 1: a uniform axial component along the trajectory direction and a radial expansion component which is assumed to be self-similar. The gas inside the cluster has an initial null velocity (like the ambient gas) but it evolves to have axial and radial components in the same manner as the drops. For a very dense cluster, momentum exchange between the drops and gas inside the cluster will rapidly reduce the relative (slip) axial velocity between the two (Bellan and Harstad, 1987a). The cluster will then act

as one large solid entity in its movement in the ambient. Note that this does not mean that radial slip is negligible. Calculation of mass loss for uncharged clusters or ambient gas ingestion for charged clusters, which are dependent on radial slip, is an important aspect of the model.

Previous results (Bellan and Harstad, 1988) have pointed out that turbulent exchange between the cluster and the surroundings are crucial during evaporation of dense clusters of drops. In the present model turbulent exchange processes are considered as well and their relative importance with respect to electrostatic effects is of interest.

Similar to previous models (Bellan and Cuffel, 1983; Bellan and Harstad, 1987a and 1988), here each drop of the cluster is considered surrounded by a a fictitious sphere of influence centered at the drop's center and having a radius which is the half distance between two adjacent drop centers. Thus the model consists of two coupled submodels: that of an individual drop in its sphere of influence and that of the multitude of interacting spheres of influence inside the cluster, as follows.

A. Model of one drop inside its sphere of influence

The classical approach is taken here whereby the radial variation of gas properties in a sphere of influence is analytically estimated using quasi-steady equations without convection, and the enhancement of evaporation due to convection is treated by multiplying the quiescent gas evaporation rate by a function of drop Reynolds number (Bellan and Harstad, 1987c). The radial variation of the drop temperature is estimated by solving the heat conduction equation within the drop and coupling it through boundary conditions to the gas phase (Bellan and Harstad, 1987c). Thus, for one drop

$$\frac{dm_d}{dt} = -4\pi R^2 \alpha_e \left(\frac{W_F}{2\pi k_G T_s} \right)^{1/2} \left[P_{sat}(T_s) - P_{Fs} \right] f_{conv} \qquad (1)$$

where f_{conv} (Re) is the convective correction and P_{Fs} is the fuel vapor partial pressure. The energy equation combined with the boundary condition yields

$$\frac{d}{dt} \left(4\pi \rho_\ell C_\ell \int_0^R T_\ell r^2 dr \right) = 4\pi R^2 Q_g + \frac{dm_d}{dt} \left[C_\ell T_s + L(T_s) \right] \qquad (2)$$

where Q_g is the heat conduction flux from the gas, $\lambda_g \partial T_g / \partial r$, at $r = R$. Note also that

$$\frac{dm_d}{dt} = 4\pi R^2 \rho_\ell \frac{dR}{dt} \qquad (3)$$

The gas temperature inside the sphere of influence, along with the corresponding heat conduction flux, is estimated by assuming that the viscosity is a function of the temperature in the same manner as in Bellan and Harstad, 1988. During the evaporation process, the composition of the gas phase changes, causing concomitant viscosity and heat capacity changes. Since the present model is directed at providing behavioral trends, not accurate quantitative predictions, this effect is neglected. The ideal gas law is used to relate gas temperature and density taking into account that the pressure is constant.

B. Model of the collection of spheres of influence

Unlike the above model which was based upon differential equations, this model is based upon global conservation equations. These describe mass, momentum and energy conservation for both phases and their interactions.

Of particular interest is the description of the radial motion of the drops in the cluster. If $\tilde{r}$ is the radial position of a drop in the cluster and $\tilde{R}(t)$ is the cluster radius, a radial similarity parameter is $\xi = \tilde{r}/\tilde{R}$, with $0 \le \xi \le 1$. For a given drop, ξ is a constant parameter. Radial velocities and the radial electric field and electrostatic force are taken proportional to ξ. (There are additional small scale electric field variations around each drop; these do not effect drop motion.) On a large length scale the charge density in a cluster is uniform. For a uniform charge, the integral form of Gauss' law gives a radial field and corresponding drop force proportional to $\tilde{r} = \xi \tilde{R}$ (t). The drop inertial force is proportional to $d^2\tilde{r}/dt^2$, or $\xi d^2\tilde{R}/dt^2$, hence both forces are linear in ξ. Global momentum equations for the radial and axial velocities are formulated in a manner similar to that of Bellan and Harstad, 1987a. The cluster boundary velocity is $d\tilde{R}/dt$, the gas expansion velocity at the cluster edge (ξ=1) is u_{ge} and the radial slip velocity is $u_{re} = d\tilde{R}/dt - u_{ge}$ at the edge of the cluster. Note that on a large length scale the evaporating drops form a uniform mass source density and that this is consistent with the similar ξu_{re} radial slip velocity. In general, the momentum equations are consistent with similarity with the exception of nonlinear drag and convective derivative terms. Average equations are formed by integrating over parameter ξ to be consistent with the other global equations where the radial dependence does not appear. (This eliminates some coupling between axial and expansion velocities due to convective derivative terms.) This means that a tendency of nonlinear drag to destroy self-similar radial motion is being neglected. The radial drag is proportional to $[C_D (u_{ra}^2 + \xi^2 u_{re}^2)^{1/2}] \xi u_{re}$. Eliminating the ξ factor in the forces, the expression in the square brackets is being averaged. In the small Reynolds number Stokes flow limit, this bracket is independent of ξ; for larger Reynolds numbers the variation is equivalent to a power of ξ

less than unity (Bellan and Harstad, 1987b; True, 1983). This averaged drag is considered adequate for the purposes of the current model, which emphasizes comparative behavior. Due to use of self-similar radial velocities, the mass loss from a cluster is calculated in a consistent manner, without the use of an assumed "trapping factor" as was done in Bellan and Harstad, 1988, where interpolation was performed from a strictly steady gas phase (maximum loss) limit to the null loss limit. This also means that the mass loss no longer depends on $d\bar{R}/dt$, which was only approximated in Bellan and Harstad, 1988. (The models produce $\bar{R}(t)$ directly, hence its derivative is not directly calculated.) In a manner similar to Bellan and Harstad, 1988, two forms of the Nusselt number are used in the model. In the first, turbulence at the edge of a dense cluster builds up with time as the cluster porosity (axial slip velocity) collapses, whereas in the second, the turbulence is initially present.

The global conservation equations are as follows:

Mass Conservation

Gas (fuel + air)

$$\frac{dm_g}{dt} = -N \frac{dm_d}{dt} + 4\pi\bar{R}^2\rho_{ga}u_{re} + \pi\bar{R}^2 (\rho_{g\infty} - \rho_{ga}) u_{ra} \qquad (4)$$

Air

$$\frac{dm_a}{dt} = 4\pi\bar{R}^2\rho_{ga} (1 - Y_{Fa}) u_{re} +$$

$$4\pi\bar{R} \frac{\mu_{g\infty}}{Pr} \left[\frac{u_g}{u_d}\right] Nuc (Y_{Fa} - Y_{F\infty}) +$$

$$\pi \bar{R}^2 \left[\rho_{g\infty} (1 - Y_{F\infty}) - \rho_{ga} (1 - Y_{Fa}) \right] u_{ra} \qquad (5)$$

where $$u_{re} = d\bar{R} / dt - u_{ge} \qquad (6)$$

$$u_{ra} = u_d - u_g \qquad (7)$$

are slip velocities.

Momentum Conservation

Drops (cluster)

$$m_d \frac{du_d}{dt} = -\frac{1}{2} \bar{\rho}_g \left[\pi R^2 C_D u_r u_{ra} + \pi \bar{R}^2 C_{Dc} \frac{m_d u_d u_g}{(N m_d + m_g)} \right] \qquad (8)$$

where $u_r^2 = u_{ra}^2 + \frac{3}{5} u_{re}^2$, u_r is the mean slip velocity magnitude, and $\bar{\rho}_g = m_g / V_c$, $V_c = 4\pi \bar{R}^3/3$. The two terms in the right hand side of eq. 8 represent respectively drag on an individual drop and drag on the entire cluster (Bellan and Harstad, 1987a)

Axial slip

$$m_d \frac{du_{ra}}{dt} = \left[\left(\frac{N m_d}{m_g} \right) \frac{dm_d}{dt} - \left(\frac{N m_d + m_g}{2 V_c} \right) \pi R^2 C_D u_r \right] u_{ra} \qquad (9)$$

Radial slip

$$m_d \frac{du_{re}}{dt} = \frac{N q_d^2}{4\pi\epsilon_o} \bar{R}^{-2} + \left[\left(\frac{N m_d}{m_g} \right) \frac{dm_d}{dt} - \left(\frac{N m_d + m_g}{2 V_c} \right) \pi R^2 C_D u_r \right] u_{re} \qquad (10)$$

Energy Conservation

Gas

$$\frac{dE_g}{dt} = -4\pi R^2 N Q_g - N \frac{dm_d}{dt} C_{pF} T_s +$$

$$4\pi\tilde{R}^2 \rho_{ga} C_p I_{ga} u_{re} + \pi\tilde{R}^2 C_p (\rho_{g\infty} T_{g\infty} - \rho_{ga} T_{ga}) u_{ra} +$$

$$4\pi\tilde{R} \frac{\mu_{g\infty}}{Pr} \left(\frac{u_g}{u_d} \right) Nuc C_p (T_{g\infty} - T_{ga}) +$$

$$\frac{6}{5} \pi\tilde{R}^2 \rho_{ga} u_{re} u_{ge}^2 - \frac{1}{2} N \frac{dm_d}{dt} u_{ra}^2 +$$

$$\frac{1}{2} \overline{\rho_g} \left[\pi R^2 N C_D u_r u_{ra}^2 + \pi\tilde{R}^2 C_{Dc} u_d u_g \left(\frac{N m_d u_d + m_g u_g}{N m_d + m_g} \right) \right] \quad (11)$$

where

$$E_g = H_g + \frac{3}{5} \frac{(Nq_d)^2}{4\pi\epsilon_0} \tilde{R}^{-1} +$$

$$\frac{3}{10} \left[N m_d (d\tilde{R}/dt)^2 + m_g u_{ge}^2 \right], \quad (12)$$

The last two lines in the right hand side of eq. 11 are small dissipation terms proportional to the square of the Mach number. Likewise, the last term in E_g is small. The derivative $d\tilde{R}/dt$ is approximated by a third order backward difference; it appears only in terms that are nearly negligible.

The total cluster gas mass, m_g, total air mass, m_a, and total thermal enthalpy, H_g, are given by

$$m_g = \rho_{ga} V_c f_s$$

$$m_a = \rho_{ga} V_c f_a$$

$$H_g = \rho_{ga} C_p T_{ga} V_c f_h$$

where f_x (R, $\bar{R}$, T_s, T_{ga}, Y_{Fs}, Y_{Fa}) are known functions of order unity (Bellan and Harstad, 1988). Since the pressure is constant, the main dependency is $H_g - V_c$. Consequently, E_g is mainly a function of $\bar{R}$ and eq. 11 may be considered as an equation for $\bar{R}$. Equations 4 and 5 determine ρ_{ga} and Y_{Fa}, hence also T_{ga}. Equations 1 and 2 determine T_s and Y_{Fs}. Equations 8, 9, 10 determine velocities. Note that the electrostatic effects appear as the first term on the right hand side of the radial slip momentum equation 10 for the electrostatic force, and the second term in equation 12 for the electrostatic field energy.

III. Results

All results presented here pertain to n-decane drops evaporating in an unvitiated ambient air. The ambient air temperature is 1000 K, the initial drop temperature is 350 K and the pressure is one atmosphere. The initial drop velocity is 5 m/s and the initial drop radius is 20 μm. The value of other parameters used in the calculation are given in Bellan and Harstad, 1987c. Similarly to Bellan and Harstad, 1988, the form of the cluster Nusselt number wherein turbulence builds up with time for dense clusters will be called turbulence model 1; turbulence is present initially for turbulence model 2.

In Figure 2, a characteristic evaporation time is shown versus initial air/fuel mass ratio for a 10 cm radius cluster with different drop charges. The time plotted is that when the drop radius decreases to 0.3 of its original size (drop mass 97.3% evaporated). The drop charge shown is relative to the mean value given by Kelly, 1984:

$$(q_d)_{max} = (7.34 \times 10^{-11} \text{ coul/cm}) R_0 \ .$$

This charge value depends only on the initial drop radius. The value apparently applies to all hydrocarbons and appears to be the maximum charge obtainable for practical sprays (Kelly, 1984). Note that for drops charged to the Kelly value, the Rayleigh charged drop shape instability occurs when the drop radius becomes somewhat smaller than 0.3 original size. The calculation is stopped as this instability is encountered, avoiding modeling of the ensuing drop breakup. Fluid dynamic forces act in concert with drop charge in the disruption of drops (Cerkanowicz, 1981). For the conditions of the present calculations, this effect is small, typically causing a reduction in the Rayleigh limit charge by less than 10%.

A spray whose initial air/fuel mass ratio is greater than or equal to 1.57 will be termed "nondense," with a corresponding maximum drop density of approximately 10^4 drops/cm^3. (This air/fuel mass ratio is 0.1 of stoichiometric.) The concept of denseness or cluster porosity directly corresponds to the relative amount of velocity slip of the ambient gas with respect to drops in the cluster. Comparison of prior and current calculations shows that for nondense clusters, the nonneglible axial slip velocity depends very weakly on the drop charge, initial cluster size, and turbulence model. In contrast, clusters having slip velocities of order 10 cm/s or less are considered dense. Thus a cluster denseness or porosity criterion based on initial air/fuel mass ratio only, independent of the above parameters, is expected to be valid. As is seen in Figure 2, only dense sprays are greatly affected by drop charging. The charge acts to expand the cluster into the hot ambient air, promoting evaporation.

The volume expansion ratio at the characteristic evaporation time is shown in Figure 3. Note that for dilute sprays the electrostatic forces are too weak to produce any significant expansion. As was shown in Bellan and Harstad, 1988,

evaporative gas cooling leads to cluster contraction for uncharged drops in dense clusters. The expansion effect of the radial evaporation flux is very weak, being proportional to the square of the small flow-Mach-number as can be seen from the terms proportional to u_{ge}^2 in eq. 12.

Prior and present calculations show that the evaporation time does not depend on the turbulence model for nondense sprays, independently of whether the drops are charged or uncharged. For dense sprays with significant charge (one quarter or more of the Kelly value), the evaporation time is slightly less with turbulence model 2, with a corresponding slightly greater volume expansion ratio. In contrast, the turbulence model can greatly affect uncharged dense sprays, as seen in Bellan and Harstad, 1988. This is due to the limited available thermal energy for evaporation in the relatively small drop interstitial region of dense sprays, along with comparitive isolation from the hot ambient. Only turbulence breaks this isolation for uncharged dense clusters, whereas charge-induced expansion into the ambient dominates for highly charged drops. For a dense spray with initial air/fuel mass ratio of 0.471, the behavior of the drop evaporation time relative to drop charge for the two turbulence models is shown in Figure 4. The time is independent of turbulence model for drop charges greater than half the Kelly value for this case. For turbulence model 1 at low drop charge, saturation before complete evaporation occurs. Table I presents a summary of the control parameters in various regimes.

The relative amount of fuel ejected from the drop cluster as a function of initial cluster size is presented in Figure 5 for an initial air/fuel mass ratio of 1.57, the dividing value for dense/nondense sprays under the initial conditions given in the first paragraph of this section. Curves are given for null and maximum drop charge for the two turbulence models. The fuel loss ratio

is an important quantity since for dense clusters ignition outside of the drop cluster is expected (Bellan and Harstad, 1987b), with only the ejected fuel participating in ignition. The fuel loss ratio depends strongly on cluster size, fairly strongly on the turbulence model, and least, but still significantly, on drop charge. Unlike the fuel loss, the calculations show that the total mass loss is nearly independent of the turbulence model, with a very weak dependence for small clusters only. Also, for charged drop clusters, the relative amount of mass entrainment of the ambient upon expansion increases with decreasing cluster size. The larger fuel loss and greater entrainment for smaller clusters may be attributed to their larger surface to volume ratio. (The curve in Figure 5 for turbulence model 1 with no charge follows an approximate inverse radius dependency).

Some limited results of charge effects on ignition are given next. For nearly dense drop clusters, with initial air/fuel mass ratio greater than or nearly equal to 1.57 but less than 5, the penetration of the ambient is small enough to allow for the possibility of a diffusive ignition criterion (Bellan and Harstad, 1987a, 1987b). In this range the ignition time decreases with increasing drop charge (drop radius at ignition increases). These effects are at most a factor of two, and largest at the higher cluster densities. Moreover, the ignition time increases as drop number density increases; dense clusters in general do not ignite before nearly complete drop evaporation (see also Bellan and Harstad, 1987b). Since the ignition time decreases with increasing drop charge the salutory effect of drop charge in reducing evaporation time may be lessened by the ignition and burning of larger drops in nearly dense clusters, which could produce an increase in unwanted byproducts such as cenospheres for multicomponent fuels which are not Diesel fuels.

Now the above results can be used to infer the effect of electrostatic charging upon soot control by using the experimental results of Sangiovanni and Liscinsky, 1984.

Despite the fact that the present calculations are made for n-decane and the results of Sangiovanni and Liscinsky, 1984, are obtained for n-hexadecane, qualitative comparisons can still be made because Figure 2 of Sangiovanni and Liscinsky, 1984, shows that although at constant initial droplet spacing the soot emission index decreases with decreasing aromatic content of the fuel, the general trend of the variation of the soot emission index with drop spacing is the same, independent of the fuel. The quantitative reduction in the value of the soot emission index with increasing drop spacing found by Sangiovanni and Liscinsky, 1984 should be considered as a minimum reduction since theirs is a single-droplet-stream experiment and thus the impact of increasing the spacing of lateral adjacent drops cannot be assessed. With this restriction in mind, the results of Fig. 2 of Sangiovanni and Liscinsky, 1984, are directly comparable to our results because the relative drop spacing here is in the same range of values as in that work. Here R_2^0 measures the same distance as Δ/d_0 in Sangiovanni and Liscinsky, 1984, which was varied there from 5 to 20. In the present calcuations for $\phi^0 = 0.471$, $T^0_{ga} = 1000$ K and $Y^0_{Fva} = 0$ the cluster is characterized by $n^0 = 3.25 \times 10^4$ cm^{-3} and $R_2^0 = 8.8$; and for $\phi^0 = 4.71$ at the same conditions, we obtain $n^0 = 2.98 \times 10^3$cm^{-3} and $R_2^0 = 19.6$. The first case corresponds to a dense cluster of drops where interactions are strong and the second case corresponds to a dilute cluster (although a rich mixture) where interactions are weak (see Fig. 2 for the uncharged limit). Although the difference between the ambient temperature used in this study and that of Sangiovanni and Liscinsky, 1984, might somewhat influence the results quantitately but not qualitatively, the conclusions should be independent of the

mass percent of ambient oxygen (in the low range) as shown in Fig. 3 of Sangiovanni and Liscinsky, 1984. Since all mass fractions must add to unity, we conclude that the results should also be independent of Y^0_{Fva} in the corresponding range. Previous results obtained for uncharged drops (Bellan and Harstad, 1988) show that the radius of the sphere of influence can either decrease for very dense clusters of evaporating drops (due to cooling effects), or remain nearly constant in the case of dilute clusters. In contrast, when charging, Fig. 3 shows that the radius of the sphere of influence, and thus that of the cluster, increases; for example when $\phi^0 = 0.471$ and the charge ratio is unity (the largest charge feasible), $R^0_2 = 8.8$ and $R_2 = 17.2$ at $R_1 = 0.3$ (the radius near Rayleigh instability). There is a continuous cluster expansion (monotonic variation) starting from the initial condition and therefore R_2 is larger than R_2^0; thus, the results of Sangiovanni and Liscinsky, 1984, can be used here uncontroversially. According to Fig. 2 of Sangiovanni and Liscinsky, 1984, an increase in R_2 from 9 to 17 (compare with the above 8.8 to 17.2) could result in a substantial decrease in the soot emission index. Since Fig. 3 shows that at constant charge the volume ratio increases with decreasing ϕ^0 (and thus R_2^0), electrostatic spray dispersion yields more dramatic results at constant charge as the cluster is denser.

IV. Summary and Conclusions

The above results show that, unlike the case of uncharged drops in dense clusters (Bellan and Harstad, 1988), when the drops are charged, turbulence is not a control parameter for dense clusters of drops; instead electrostatic effects dominate. For dilute clusters of drops it is found that similarly to the uncharged drops (Bellan and Harstad, 1988), turbulence effects are unimportant. Significantly, the results above show that the evaporation time of dilute clusters of drops cannot be changed by charging the drops in contrast to the dense clusters of drops where the evaporation time can be considerably shortened by this procedure. Moreover, it is also found that the fuel vapor loss from the cluster increases as turbulence increases and as cluster size and/or charge decreases.

It was also shown by comparing with existing experimental results that when charging the drops with the maximum empirical limit obtained by Kelly, 1984, substantial decrease in the soot emission index can be achieved for dense clusters of drops. These results are encouraging and further studies of electrostatic spray dispersion should be made in order to ascertain its full range of posibilities.

Acknowledgment

This work was sponsored by the Army Research Office and the U. S. Department of Energy through an arrangement with the National Aeronautics and Space Administration. The respective Program Managers were Dr. David Mann and Mr. Marvin Gunn, the latter Manager of the Energy Conversion and Utilization Technologies Program.

Nomenclature

Symbols

a	radius of the sphere of influence of each drop
C_D, C_{Dc}	drag coefficients for drop, cluster
C_ℓ	liquid specific heat
C_p, C_{pF}	specific heat of gas, fuel
H_g	total enthalpy of cluster
k_G	universal gas constant
L	latent heat of evaporation of fuel
m	mass
n	drop number density
N	number of drops
Nuc	Nusselt number of cluster
p	pressure
Pr	Prandtl number
q_d	drop charge
r	radial coordinate
R	drop radius
$\tilde{R}$	cluster radius
R_1	R/R^o
R_2	a^o/R^o
Re	Reynolds number of a drop
t	time
T	temperature
u	velocity
u_{ge}	gas expansion velocity at cluster edge
u_{ra}	axial slip velocity
u_{re}	expansion slip velocity
V_c	cluster volume
W_F	fuel molar weight
Y_{Fa}	interstitial fuel mass fraction
$Y_{F\infty}$	ambient fuel mass fraction

Greek Symbols

α_e	evaporation accomodation coefficient
ϵ_0	permittivity of free space
λ_g	gas thermal conductivity
$\mu_{g\infty}$	ambient viscosity
ρ	mass density
ϕ	air fuel, mass ratio

Subscripts

a	drop interstitial region
d	drop
g	gas in cluster
ga	interstitial region gas
g_∞	ambient gas
ℓ	liquid
r	relative or slip velocity
s	drop surface

Superscripts

o	initial condition

References

Ahmad, T., Speck, C. E., and Sing, D. C., "Effect of Electric Fields Applied within the Prechamber on Particulate Emissions from a Diesel Engine," GMR-3326 Report, 1980.

Bellan, J., "A New Approach to Soot Control in Diesel Engines by Fuel-Drop Charging," Combust. Flame, 51, 117-119, 1983.

Bellan, J. and Cuffel, R., "A Theory of Non Dilute Spray Evaporating Based Upon Multiple Drop Interactions," Comb. Flame, 51, 1, 55-67, 1983.

Bellan, J. and Harstad, K., "The Details of the Convective Evaporation of Dense and Dilute Clusters of Drops," Int. J. Heat Mass Transfer, 30, 6, 1083-1093, 1987a.

Bellan, J. and Harstad, K., "Ignition of Non Dilute Clusters of Drops in Convective Flows," Combust. Sci. and Tech., 53, 75-87, 1987b.

Bellan, J. and Harstad, K., "Analysis of the Convective Evaporation of Nondilute Clusters of Drops," Int. J. Heat Mass Transfer, 30, 1, 125-136, 1987c.

Bellan, J. and Harstad, K , "Turbulence Effects During Evaporation of Drops in Clusters," Int. J. Heat Mass Transfer, 31, 8, 1655-1668, 1988.

Cerkanowicz, A. E., "Rayleigh Limit for Nonstationary Charged Drops," IEEE/IAS Annual Meeting, Philadelphia, PA, October, 1981, IEEE/IAS Conference Record 81CH1678-2.

Kelly, A. J., "The Electrostatic Atomization of Hydrocarbons," J. of the Inst. of Energy, 312-320, 1984.

Mayo, P. M. and Weinberg, F. J., "On the Size, Charge and Number-rate of Formation of Carbon Particles in Flames Subjected to Electric Fields," Proc. Roy. Soc. Lond., A 319, 351, 1970.

Prado, G. P., Lee, M. L., Hites, R. A., Hoult, D. P. and Howard, J. B., "Soot and Hydrocarbon Formation in a Turbulent Diffusion Flame," Proc. 16th Symp. (Int.) on Combustion, 649-661, 1977.

Roth, D. G. and Kelly, A. J., "Analysis of the Disruption of Evaporating Charged Droplets, IEEE Transactions on Industry Applications, IA-19, 5, 771-775, 1983.

Thong, K. C. and Weinberg, F. J., "Electrical Control of the Combustion of Solid and Liquid Particulate Suspensions," Proc. Roy. Soc. Lond., A 324, 201-215, 1971.

True, M. A., "Modelling of Electrostatic Spray Plumes," IEEE/IAS Annual Meeting, 1980; IAS Transactions, 993-997, 1983.

Sangiovanni, J. J. and Liscinsky, D. S., "Soot Formation Characteristics of Well-Defined Spray Flames," Proc. of the 20th Symp. (Int.) on Combustion, 1063-1073, 1984.

TABLE 1

Control Parameters for the Evaporation Time

Control Parameter for the Evaporation Time	Uncharged drops[a]		Charged drops	
	dense	non-dense	dense	non dense
Turbulence	important	not important	not important	not important
Electrostatic charge when $q_d > \frac{(q_d)_{max}}{4}$	---	---	important	not important

(a) Bellan and Harstad, 1988.

Figure Captions

Fig. 1 Moving Spherical Cluster.

Fig. 2. Characteristic evaporation time vs initial air/fuel mass ratio. Drop charge is relative to maximum, see text.

Fig. 3. Volume expansion ratio vs initial air/fuel mass ratio. Drop charge is relative to maximum.

Fig. 4. Characteristic evaporation time vs ratio of drop charge relative to maximum. Spray cluster is dense, see Bellan and Harstad, 1988, for turbulence models.

Fig. 5 Relative fuel ejection from cluster vs initial cluster radius. Cluster density is at the boundary of the near-dense/nondense regimes.

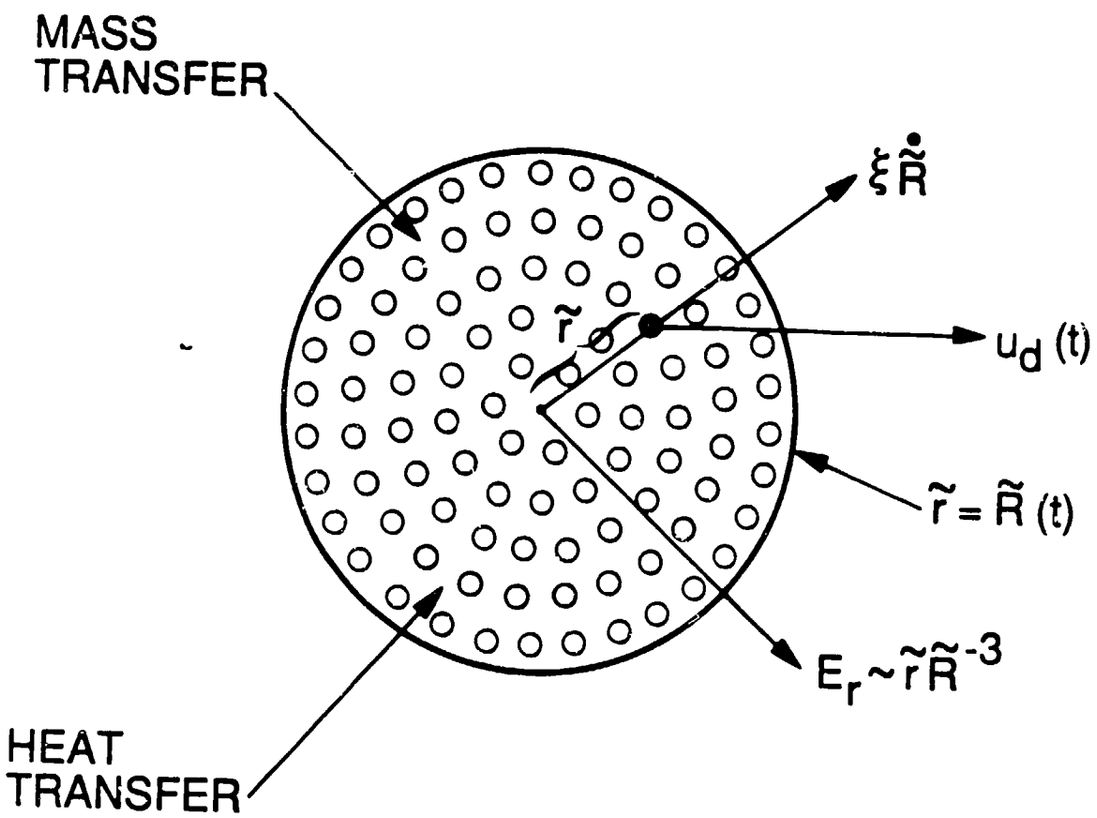
MASS
TRANSFER
$\xi \dot{\tilde{R}}$
$\tilde{r}$
u_d (t)
$\tilde{r} = \tilde{R}$ (t)
$E_r \sim \tilde{r}\tilde{R}^{-3}$
HEAT
TRANSFER

Figure 1

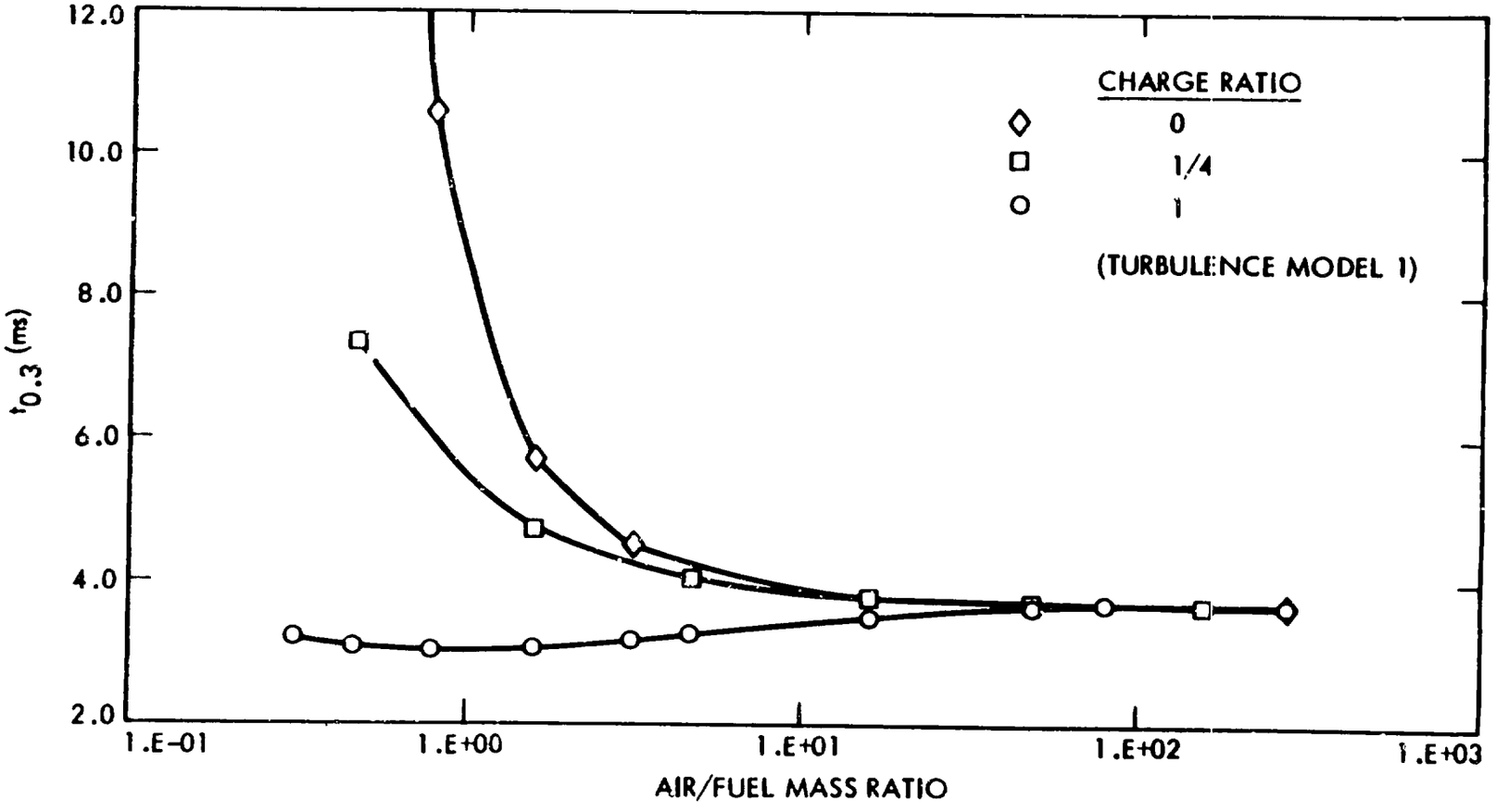
12.0
10.0
8.0
6.0
4.0
2.0
$t_{0.3}$ (ms)
1.E-01
1.E+00
1.E+01
1.E+02
1.E+03
AIR/FUEL MASS RATIO
CHARGE RATIO
0
1/4
1
(TURBULENCE MODEL 1)

Figure 2

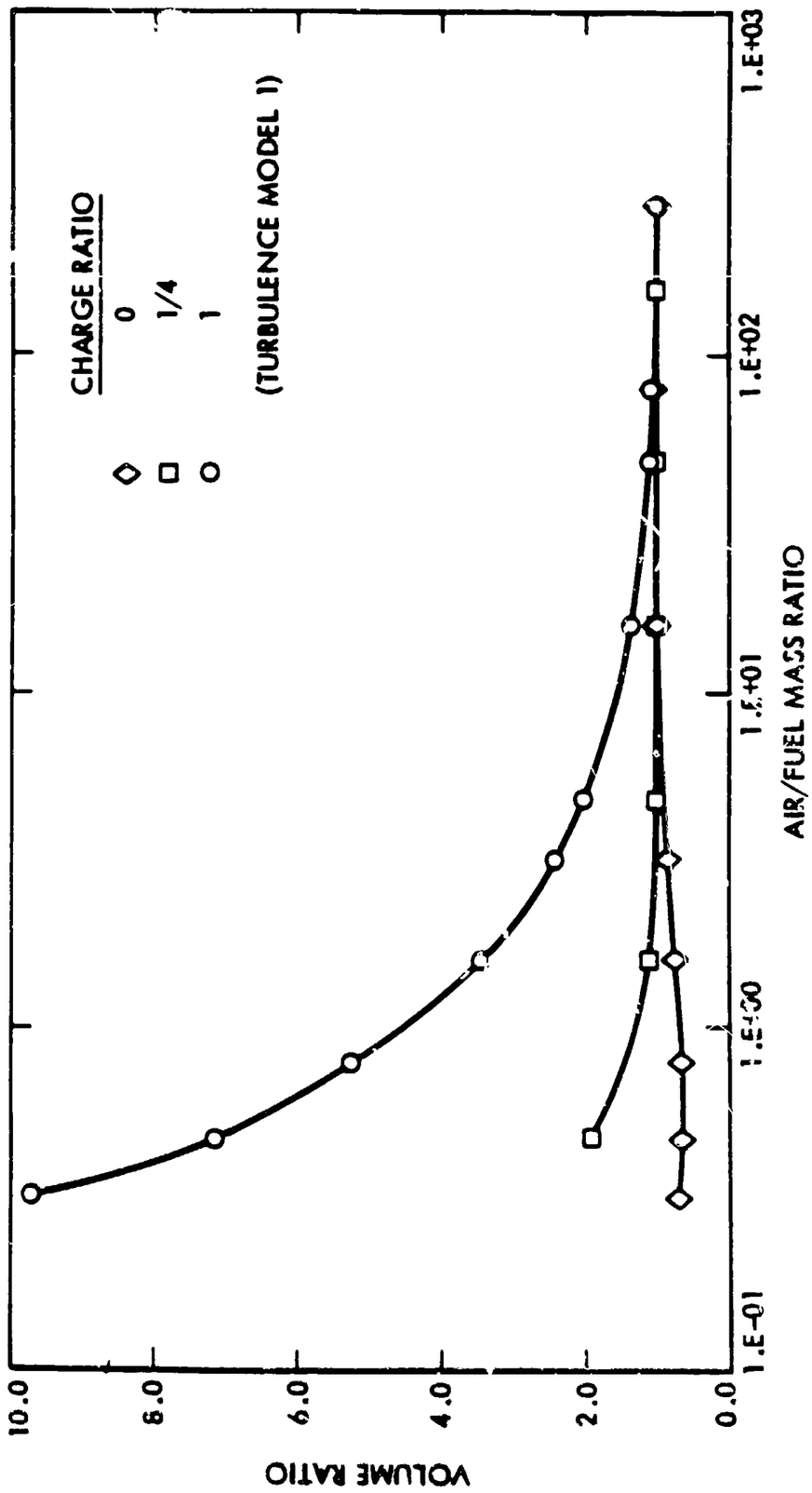
CHARGE RATIO
0
1/4
1
(TURBULENCE MODEL 1)
VOLUME RATIO
10.0
8.0
6.0
4.0
2.0
0.0
1.E-01
1.E+00
1.E+01
1.E+02
1.E+03
AIR/FUEL MASS RATIO

Figure 3

◇ TURBULENCE MODEL 1
○ TURBULENCE MODEL 2
ϕ = 0.471
$t_{0.3}$ (ms)
15.0
10.0
5.0
0.00
0.0
0.20
0.40
0.60
0.80
1.00
CHARGE RATIO

Figure 4

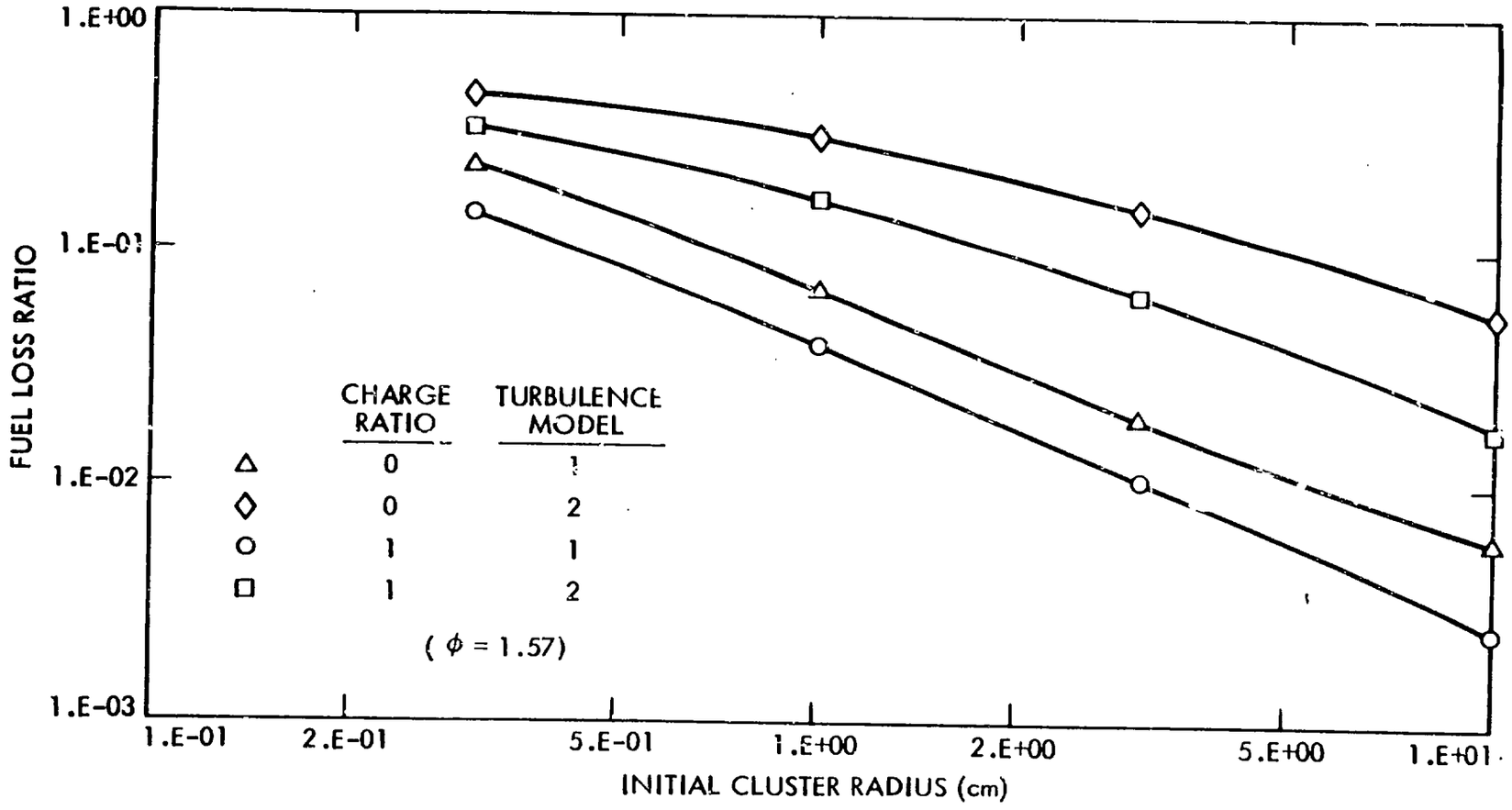
1.E+00
1.E-01
1.E-02
1.E-03
FUEL LOSS RATIO
CHARGE RATIO
TURBULENCE MODEL
0
1
0
2
1
1
1
2
(ϕ = 1.57)
1.E-01
2.E-01
5.E-01
1.E+00
2.E+00
5.E+00
1.E+01
INITIAL CLUSTER RADIUS (cm)

Figure 5